Search for triple Higgs boson production in the *6b* final state using *pp* collisions at $\sqrt{s} = 13$ TeV with the ATLAS detector

G. Aad *et al.*[*]

(ATLAS Collaboration)

A search for the production of three Higgs bosons (HHH) in the $b\bar{b}b\bar{b}b\bar{b}$ final state is presented. The search uses 126 fb^{-1} of proton-proton collision data at $\sqrt{s} = 13$ TeV collected with the ATLAS detector at the Large Hadron Collider. The analysis targets both nonresonant and resonant production of HHH. The resonant interpretations primarily consider a cascade decay topology of $X \to SH \to HHH$ with masses of the new scalars X and S up to 1.5 and 1 TeV, respectively. In addition to scenarios where S is off-shell, the nonresonant interpretation includes a search for Standard Model HHH production, with limits on the trilinear and quartic Higgs self-coupling set. No evidence for HHH production is observed. An upper limit of 59 fb is set, at the 95% confidence level, on the cross section for Standard Model HHH production.

I. INTRODUCTION

Since the discovery of the 125 GeV Higgs boson (H) [1,2] at the Large Hadron Collider's (LHC) ATLAS and CMS experiments, a core part of the LHC research program has been to investigate the properties of the Higgs boson and establish if they are in agreement with the predictions of the Standard Model (SM) [3,4]. Two key parts of the SM Higgs mechanism are the trilinear (λ_3) and quartic (λ_4) self-coupling constants, which are a crucial part of the electroweak symmetry breaking mechanism and determine the shape of the Higgs field potential. Higgs self-coupling modifiers κ_3 and κ_4 are introduced using the κ framework, in which they are defined as $\kappa_i = \lambda_i/\lambda_i^{\text{SM}}$ for $i = 3$, 4, such that $\kappa_i = 1$ corresponds to the couplings predicted by the SM [5]. Combinations of searches for di-Higgs production constrain κ_3 (also often referred to as κ_λ) to be between -1.2 and 7.2 at the 95% confidence level (CL) [3,4,6]. The most recent combination of results for single- and di-Higgs production further constrains κ_3 to be between -0.4 and 6.3 (when other Higgs boson couplings are assumed to have their SM values) [7]. However, there have been no experimental constraints on λ_4 or its relation to λ_3 prior to the results presented in this paper. Searches for HHH production have been proposed in Refs. [8,9], which specifically identify the six b-jet final state as a suitable channel and explore the possibility of constraints on λ_4 and λ_3. A recent comprehensive white paper [10] explores additional channels and identifies key challenges for future HHH searches.

This paper presents searches for the simultaneous production of three Higgs bosons—tri-Higgs (HHH)—in the six b-jet final state. Data collected during Run 2 of the LHC by the ATLAS experiment [11] between 2016 and 2018 are used. As well as a unique dependence on λ_4 and a dependence on λ_3, HHH provides new sensitivity to Beyond SM (BSM) physics with extended scalar sectors. The results are interpreted in terms of three benchmark models.

First, SM-like scenarios are considered to place constraints on the Higgs self-coupling modifiers κ_3 and κ_4. All leading-order gluon-gluon fusion (ggF) production modes represented in Fig. 1 are included.

Second, scenarios extending the SM by adding two real scalar bosons X and S are probed, which are hypothesized in several BSM models. The mass ranges $325 < m_X < 575$ GeV and $200 < m_S < 350$ GeV are considered and, by convention, $m_X > m_S$. In this interpretation, the mass ranges are chosen to fulfill perturbative unitarity bounds [12]. The scenarios include cases in which either resonant or nonresonant production is dominant. All leading-order ggF production modes (illustrated in Fig. 1) are considered, including interference between all diagrams, both BSM and SM. Models including the two real scalar model (TRSM) [12,13] and a "simple model for dark matter and *CP* violation" (DM-CPV) [14] feature this extension to the SM. For suitable parameter choices, the HHH production cross section is preferentially enhanced without increasing single- or di-Higgs production beyond experimental constraints. Negligible differences are found in the HHH event kinematics between the TRSM

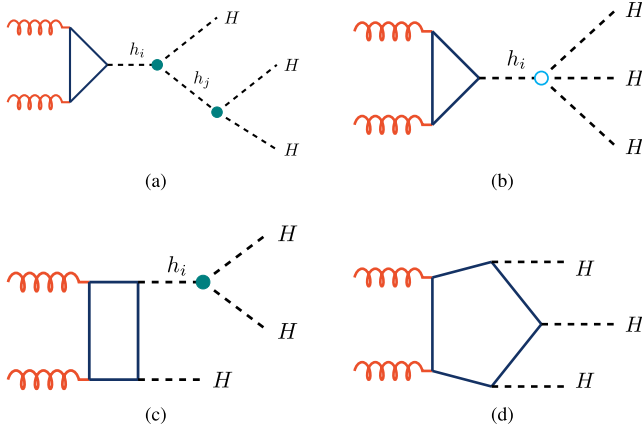[*]Full author list given at the end of the article.

FIG. 1. Leading-order Feynman diagrams for gluon-gluon fusion triple Higgs boson production. The symbols h_i and h_j represent any of the SM Higgs H or heavy scalars, X and S. The resonant cascade decay is shown in (a), direct resonant triple Higgs production is shown in (b), resonant di-higgs production in association with a single Higgs boson is shown in (c) and fully non-resonant production is shown in (d). For the case where $h_i = h_j = H$, the solid circle indicates the trilinear self-coupling λ_3, and the open circle indicates the quartic-linear self-coupling λ_4.

and DM-CPV models, so Monte Carlo (MC) simulated events are generated only in the TRSM, as described in Sec. III, and results are interpretable in both models.

Finally, scenarios with resonant production of generic heavy spin-0 bosons X and S are also considered, with masses $m_X > m_S$, covering $550 < m_X < 1500$ GeV and $275 < m_S < 1000$ GeV. The search covers benchmark scenarios in which both particles have either a narrow or wide decay width, with resonances that have a width below or just above the detector resolution, respectively. Only resonant ggF production [Fig. 1(a)] is chosen for consideration to give a simplified treatment and avoid the large contributions from nonresonant diagrams at leading order in the TRSM. This interpretation allows the search to probe generically for resonances that lie beyond the masses permitted by the TRSM benchmark.

To enable these interpretations, the analysis is divided into three searches based on the kinematics of the signal models considered: "nonresonant," "resonant," and "heavy resonant." The nonresonant search is used for the TRSM parameter space dominated by nonresonant production and the SM-like interpretation, the resonant search is used for the TRSM parameter space dominated by resonant production, and the heavy-resonant search is used for the generic heavy-resonance signal models. Each search follows the same general analysis strategy. Deep neural network (DNN) classifiers are trained to discriminate between the relevant signals and the SM background. The dominant SM background process in all searches is the quantum chromodynamics (QCD) multijet production, which is estimated by using an entirely data-driven approach based on an extrapolation between different

b-jet multiplicities. To obtain the final results in each search, a profile likelihood fit is performed over the binned DNN score distribution.

The structure of this paper is as follows. In Sec. II, the ATLAS detector is described, followed by a summary of the data and MC simulated events used in Sec. III. Section IV explains how events are reconstructed, and Sec. V explains the analysis strategy and how signal events are selected. In Sec. VI, the estimate of the SM background is described, followed by an explanation of the statistical interpretation in Sec. VII. A summary of the uncertainties considered is presented in Sec. VIII and, finally, the results and conclusions are provided in Secs. IX and X, respectively.

II. ATLAS DETECTOR

The ATLAS experiment [11] at the LHC is a multipurpose particle detector with a forward–backward symmetric cylindrical geometry and a near 4π coverage in solid angle.[1] It consists of an inner tracking detector (ID) surrounded by a thin superconducting solenoid providing a 2T axial magnetic field, electromagnetic and hadronic calorimeters, and a muon spectrometer. The inner tracking detector covers the pseudorapidity range $|\eta| < 2.5$. It consists of silicon pixel, silicon microstrip, and transition radiation tracking detectors. Lead/liquid-argon (LAr) sampling calorimeters provide electromagnetic (EM) energy measurements with high granularity within the region $|\eta| < 3.2$. A steel/scintillator-tile hadronic calorimeter covers the central pseudorapidity range ($|\eta| < 1.7$). The end cap and forward regions are instrumented with LAr calorimeters for EM and hadronic energy measurements up to $|\eta| = 4.9$. The muon spectrometer (MS) surrounds the calorimeters and is based on three large superconducting air-core toroidal magnets with eight coils each. The field integral of the toroids ranges between 2.0 and 6.0 T m across most of the detector. The muon spectrometer includes a system of precision tracking chambers up to $|\eta| = 2.7$ and fast detectors for triggering up to $|\eta| = 2.4$. The luminosity is measured mainly by the LUCID-2 [15] detector, which is located close to the beam pipe. A two-level trigger system is used to select events [16]. The first-level (L1) trigger is implemented in hardware and uses a subset of the detector information to accept events at a rate below 100 kHz. This is followed by a software-based trigger (HLT) that reduces the accepted event rate to 1 kHz on average depending on the data-taking

---

[1]ATLAS uses a right-handed coordinate system with its origin at the nominal interaction point (IP) in the center of the detector and the z-axis along the beam pipe. The x-axis points from the IP to the center of the LHC ring, and the y-axis points upwards. Polar coordinates (r, ϕ) are used in the transverse plane, with ϕ being the azimuthal angle around the z-axis. The pseudorapidity is defined in terms of the polar angle θ as $\eta = -\ln\tan(\theta/2)$ and is equal to the rapidity $y = \frac{1}{2}\ln(\frac{E+p_z}{E-p_z})$ in the relativistic limit. Angular distance is measured in units of $\Delta R \equiv \sqrt{(\Delta y)^2 + (\Delta\phi)^2}$.

conditions. A software suite [17] is used in data simulation, in the reconstruction and analysis of real and simulated data, in detector operations, and in the trigger and data acquisition systems of the experiment.

III. DATA AND MONTE CARLO SIMULATIONS

A. Data and triggers

The proton-proton (pp) collisions used in this paper were collected between 2016 and 2018, at a center-of-mass energy of $\sqrt{s} = 13$ TeV. They correspond to an integrated luminosity of 126 fb^{-1}, with an uncertainty of 0.84% [18] obtained using the LUCID-2 detector for the primary luminosity measurements, complemented by measurements using the inner detector and calorimeters. Only events that satisfy data quality requirements that ensure the stable operation of the ATLAS detector [19] were considered.

Events from each year satisfy triggers requiring multiple jets and b-tagged jets [20], which were implemented in 2016. These jets were reconstructed using the anti-k_t algorithm with radius parameter $R = 0.4$ [21,22]. Jets originating from b-quarks were tagged using the MV2c20 (MV2c10) algorithm in 2016 (2017–2018) [20] operating at a 60%–70% identification efficiency, as measured using simulated $t\bar{t}$ events. For all years, the triggers used required four jets with transverse momentum $p_T > 15$ GeV and $|\eta| < 2.5$ at the L1 level. In 2016 and 2018, the trigger used required two b-tagged jets and two additional jets at the HLT level, all with $p_T > 35$ GeV ($2b + 2j$). In 2017, a trigger requiring three b-tagged jets and one additional jet at the HLT level, all with $p_T > 35$ GeV ($3b + 1j$), was used instead. The triggers selected maximize the efficiency for the resonant (m_X, m_S) phase space within the TRSM perturbative unitarity bounds. Different triggers were used in different years due to changes in the online b-tagging working points. Depending on the mass point and data-taking year, the triggers used were 90%–98% efficient. During 2016, a fraction of the data taking (8.3 fb^{-1}) was affected by an inefficiency in the trigger-level vertex reconstruction, which reduced the efficiency of the algorithms used to identify b-tagged jets; those events were not retained for further analysis.

B. Signal models and event simulation

For all signal samples described in this section, MC simulated signal events are generated using MadGraph [23] 2.9.5 at leading order in the strong coupling constant, using the NNPDF3.0NLO parton distribution function (PDF) set [24] with the A14 set of tuned parameters (tune) [25]. The $H \to b\bar{b}$ branching fraction is taken to be 0.582, and its total width is 4.088 MeV, corresponding to the SM values for a Higgs boson mass of 125 GeV [26]. All events are showered with Pythia 8.245 [27], and a generation-level filter

requiring at least four b-tagged[2] jets with $p_T > 25$ GeV is applied.

For the SM-like interpretation in the nonresonant search, a single sample is generated at $(\kappa_3, \kappa_4) = (1, 1)$. All diagrams in Fig. 1 are included, fully accounting for interference between them. The Higgs bosons are decayed exclusively to $b\bar{b}$. A reweighting [28] allows the sample kinematics to be altered to reflect different values of κ_3 and κ_4, which follows a similar procedure to that outlined in Ref. [29]. The SM HHH ggF production cross section at a center-of-mass energy of $\sqrt{s} = 13$ TeV is taken as $\sigma_{HHH}^{SM} = 0.079^{+0.012}_{-0.013}$ fb at next-to-next-to-leading-order (NNLO), calculated by extrapolating cross sections at higher $\sqrt{s}$ values presented in Ref. [30] and including uncertainties from missing higher-order corrections ($+5\%, -8\%$) and the finite top quark mass approximation ($\pm 15\%$).

For the resonant and nonresonant searches, benchmark 3 of the TRSM, defined in Ref. [12], is used for signal generation.[3] Here, the SM is extended by two neutral CP-even scalars, X and S. Interactions between X/S and non-Higgs SM particles come via the mixing between the X/S fields and the SM Higgs field, making the couplings proportional to the SM-Higgs couplings. Here, by choice, $m_X \geq m_S \geq m_H$. The benchmark chosen sets the TRSM parameters to maximize HHH production through a resonant cascade decay $gg \to X \to HS \to HHH$, though all possible leading-order $gg \to HHH$ diagrams are generated together with interference. Typical values for the branching fractions $X \to SH$ and $S \to HH$ are 45% and 70%, respectively. For more information, see Ref. [12].

For the TRSM signals, the Higgs bosons are decayed inclusively using Pythia 8.245 [27]. A set of 27 (m_X, m_S) points are chosen within the perturbative unitarity bounds of the TRSM, with $325 \leq m_X \leq 575$ GeV and $200 \leq m_S \leq 350$ GeV. This includes two categories: 19 "resonant" points, where $m_X > m_S + m_H$ and $m_S > 2m_H$, such that the resonant cascade decay is on-shell and dominant, and eight "nonresonant" points, where $m_S \leq 2m_H$, such that the resonant cascade is off-shell and nonresonant diagrams become dominant.

The results of the resonant and nonresonant searches can also be interpreted in the DM-CPV model, presented in Ref. [14], using benchmarks 1 and 3 defined therein. These benchmarks are defined to maximize HHH production and can be extended across the same (m_X, m_S) plane as the TRSM. In the nomenclature of Ref. [14], $X = h_3$ and $S = h_2$.

---

[2]At the truth level, b-tagged jets are defined as jets which have a b-hadron of $p_T > 5$ GeV lying within a cone of size $\Delta R = 0.3$ from their axis.

[3]A more recent benchmark satisfying additional constraints from the electroweak phase transition is presented in Ref. [31], but the kinematic differences between the new benchmark and the one used here are minimal.

For the heavy-resonant search, more generic benchmark models are considered, to represent a broader class of possible BSM models to which this analysis is sensitive. The TRSM benchmark 3 is used as a starting point, but only the cascade resonance decay [Fig. 1(a)] is generated. The widths of the X and S particles are set to 1% (20%) of their masses, to define narrow (wide)-width signal models. These modifications lead to generic signal samples that no longer represent the TRSM.

The generic heavy-resonant signals are generated similarly to the other models, but using MadSpin [32] for the $S \to HH$ decay. The Higgs bosons are decayed exclusively to $b\bar{b}$. At each width, 45 samples are produced, with $550 \leq m_X \leq 1500$ GeV and $275 \leq m_S \leq 1000$ GeV.

For all generated signal events, the detector response is simulated [33] using a fast parametrized simulation of the calorimeters [34], and the full Geant4 [35] simulation for the other subdetectors. Events are processed using the same reconstruction software used for the data. The effect of multiple interactions in the same and neighboring bunch crossings (pile-up) is modeled by overlaying the simulated hard-scattering event with inelastic pp events generated with Pythia 8.186 [36] using the NNPDF2.3LO PDF set [37] and the A3 set of tuned parameters [38].

IV. EVENT RECONSTRUCTION

For proton-proton collision events, primary vertices are reconstructed using at least two charged-particle tracks with $p_T > 500$ MeV, measured in the ID [39]. The primary vertex with the largest sum of squared track momenta is assigned as the hard-scatter vertex.

Hadronic jets are reconstructed from particle flow objects [40] using the anti-k_t algorithm with a radius parameter of $R = 0.4$. These are calibrated using a multi-step procedure, as outlined in Ref. [41]. Jets are required to have $p_T > 20$ GeV and $|\eta| < 2.5$. To suppress jets originating from pile-up, a neural-network-based jet vertex tagger (NNJVT) is used, which is an updated version relative to the likelihood-based algorithm described in Ref. [42]. Jets with $20 < p_T < 60$ GeV are required to satisfy a selection on the NNJVT with a 0.88–0.99 probability of correctly identifying hard-scatter jets depending on the p_T, as evaluated in $Z(\to \mu\mu) +$ jet events with a mean of 33.7 interactions per bunch crossing. Outside of this p_T range, no NNJVT requirement is applied.

Jets originating from b-quarks are identified using a DNN-based algorithm (DL1d) [43–45]. The identification requirement used selects jets with $p_T > 20$ GeV containing b-hadrons, with an efficiency of 77%, and has a probability of 0.38% (15.5%) of misidentifying light-flavor (charm) jets, as determined in a sample of simulated $t\bar{t}$ events. The b-tagging efficiencies in simulated events are corrected to match those measured in data [46–48]. Uncertainties related to the flavor-tagging selections are described in Sec. VIII.

To account for energy lost to muons in semileptonic b-hadron decays, a momentum correction [49] is applied. For this purpose, muons are reconstructed. Muon candidates are found by matching ID tracks with either MS tracks or aligned individual hits in the MS and performing a combined track fit [50]. They are required to have $p_T > 4$ GeV, $|\eta| < 2.5$, and to satisfy the Medium identification criteria defined in Ref. [50]. If any muons are within a cone of $\Delta R = \min(0.4, 0.04 + 10/p_T^\mu \text{ [GeV]})$ around the jet axis, their four-momentum is added to that of the jet. Additionally, the energy in the calorimeter deposited by the muons (computed according to Ref. [51]) is subtracted from the jet to avoid double counting.

Corrections are applied to all signal MC simulated events to account for differences observed between the jet trigger efficiencies in data and simulation. These corrections (scale factors, SFs) are calculated from the ratios of event-level jet trigger efficiencies in data and MC, which are in turn constructed from per-jet trigger efficiencies. The efficiencies are estimated in $t\bar{t}$ MC simulated events and data satisfying a $t\bar{t}$-like event selection, with at least one top quark decaying leptonically, and collected using triggers requiring one muon and one jet to obtain an unbiased sample enriched in b-jets. The $t\bar{t}$ events are simulated using Powheg Box v2 [52–55] at next-to-leading-order (NLO) with the NNPDF3.0nlo [24] PDF set and A14 tune [25]. Pythia 8.230 [27] is used to model the parton shower, hadronization, and the underlying event. Separate SFs are estimated for the L1 and HLT, and for each jet as a function of p_T.

For each of the jets in the event selection, and for each data-taking year, the L1 trigger per-jet efficiencies are calculated. The efficiency is defined as the fraction of the n-th p_T-ordered jets geometrically matched[4] to an L1 jet and passing the L1 trigger threshold in that year. Similarly, the HLT per-jet efficiencies are calculated as the fraction of these L1-trigger-passing n-th jets that are geometrically matched to an HLT jet and pass the HLT trigger threshold in that year. The L1 and HLT per-jet efficiencies are both calculated in bins of jet p_T. These are combined to give overall event-level L1 and HLT jet trigger efficiencies, accounting for the combinatorial possibilities of selecting four jets that fired the trigger in events with more than four jets. The L1 and HLT SFs are then calculated and multiplied to provide an overall SF for each event.

V. ANALYSIS STRATEGY

A. Event selection and strategy overview

To be considered in the analysis, all data and MC simulated events must satisfy the trigger requirements defined in Sec. III A and a set of preselection requirements, now described. At least six jets are required, with at least

---

[4]The geometric matching requires $\Delta R < 0.4$ between the reconstructed and trigger-level jets.

four having $p_T > 40$ GeV in line with the trigger requirements. At least four jets must be b-tagged.

The analysis further categorizes events into three orthogonal regions, based on the multiplicity of b-tagged jets. Denoted $4b$, $5b$, and $6b$, respectively, these regions are defined to satisfy the preselection and required to have exactly four, exactly five, or at least six b-tagged jets. The $6b$ region is enriched in the signal processes and is also referred to as the signal region (SR). The $5b$ and $4b$ regions are control regions (CRs) enriched in background processes and are used to derive the $6b$ background estimate. The overall acceptance times efficiency for the SM signal (for which only the $H \to bb$ decay is considered) to fall into the $6b$ region is 5.5%. For the $4b$ and $5b$ regions, the acceptance times efficiency is 27% and 17%, respectively.

The general analysis strategy is the same for each of the three searches: nonresonant, resonant, and heavy resonant. In each case, a DNN classifier is trained to discriminate between the signal models and the SM background, which is dominated by multijet production. A profile likelihood fit is performed over the binned DNN score distribution to obtain the final results.

The kinematic properties of the reconstructed Higgs boson candidates provide important input features for the DNNs. A mass-based pairing algorithm is used to assign jets to each of three Higgs boson candidates, as described in Sec. V B.

A fully data-driven background estimate is used for the analysis. The approach assumes that the kinematic properties of the background processes are similar between events with four, five, or six identified b-jets in the final state. Systematic uncertainties arising from this approach and its core assumption are discussed in Sec. VIII. The background estimate in the $6b$ search region is obtained by extrapolating each DNN score distribution in data from the $4b$ and $5b$ regions. Both the $5b$ and $6b$ regions are included in the fit.

Figure 2 shows a diagram of the different regions in the analysis and how they are used in the final fit. Each DNN score distribution is divided into three regions. The "high-score" region contains 90% of the combined yields of the relevant signal samples and provides the bulk of the analysis sensitivity in the fit. The "low-score" region is enriched in background, and it is used to constrain the background estimate in the fit as well as to derive systematic uncertainties on it. The low-score $4b$ data are used in the systematic uncertainty estimate but are not included in the final fits, preventing any double counting of degrees of freedom. The "excluded" region lies below the low-score region and is defined as the region in which the DNN score distribution extrapolation fails to model the observed $6b$ data within one standard deviation of the statistical uncertainty. Discarding the excluded region reduces the size of the systematic uncertainties arising from the small differences in kinematics between the remaining low- and high-score regions.

B. Higgs boson reconstruction

To reconstruct the three Higgs boson candidates in signal events, which is useful to help discriminate between the signals and background, the six jets from the Higgs decays (labeled jets $a - f$) must be selected and paired. Pairing is performed on all events satisfying the preselection requirements. In the case of $6b$ events, the six jets to pair are the six highest p_T b-tagged jets. For $4b$ ($5b$) events, the six jets to pair are all of the b-tagged jets, plus the two (one) highest p_T non-b-tagged jets.

The pairing algorithm used is defined by minimizing

$$|m_{H1} - 120 \text{ GeV}| + |m_{H2} - 115 \text{ GeV}| + |m_{H3} - 110 \text{ GeV}|, \quad (1)$$
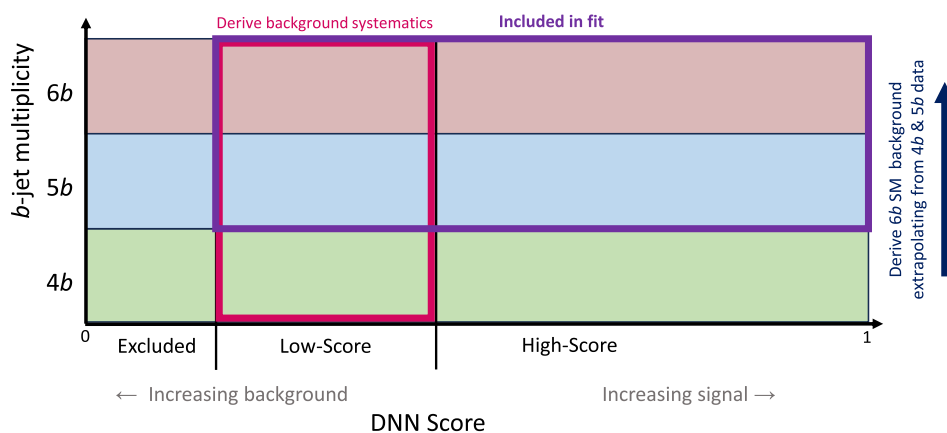

FIG. 2. A schematic diagram of the analysis strategy and regions. The strategy is the same for each DNN, although the precise selections defining the excluded, low-score, and high-score regions differ. The procedure to form the $6b$ background estimate by extrapolating from data in the $4b$ and $5b$ regions is described in Sec. VI.

over all possible permutations of jet pairs (for jets $a - f$) that satisfy the following transverse-momentum constraints:

$$p_T^{ab} > p_T^{cd} > p_T^{ef}, \quad \text{where } p_T^{H1} = p_T^{ab},$$
$$p_T^{H2} = p_T^{cd}, \quad \text{and} \quad p_T^{H3} = p_T^{ef}.$$

The numeric constants in Eq. (1) are chosen based on the peaks of the m_{Hi} distributions in simulated signal events. These differ from the observed Higgs boson mass of 125 GeV due to detector effects, energy lost to neutrinos from the b-hadron decays, and out-of-cone radiation.

The performance of the pairing algorithm is assessed using the pairing efficiency, which is defined as the fraction of signal events that are correctly paired out of all events where a correct pairing is possible. Correct pairing may not be possible if the jets cannot all be geometrically matched to truth-level b-quarks from each Higgs boson decay. This

can occur if any of the six jets fall out of the tracker acceptance ($|\eta| > 2.5$), or if two b-quarks are close enough together that they are matched to the same jet. The correct pairing is defined using a geometric matching between MC truth jets (reconstructed using the anti-k_t algorithm with $R = 0.4$ on stable, final-state particles from MC generators) and reconstructed jets. Correct pairing is possible in 74%–84% of BSM signals, depending on m_X and m_S. The pairing efficiencies for each signal model parameter plane are shown in Fig. 3. In scans over the (m_X, m_S) space, the pairing efficiency is calculated at each simulated mass point and a cubic interpolation using the nearest four points is used. For the scan of the (κ_3, κ_4) space, a parametric reweighting is used and, therefore, an arbitrarily smooth evaluation of pairing efficiency is achieved. A correct pairing is possible in 81% of SM signal events, and the pairing efficiency is 61%. The change in pairing efficiencies over the signal planes is a result of changing kinematics—the higher the p_T of the Higgses, the easier the
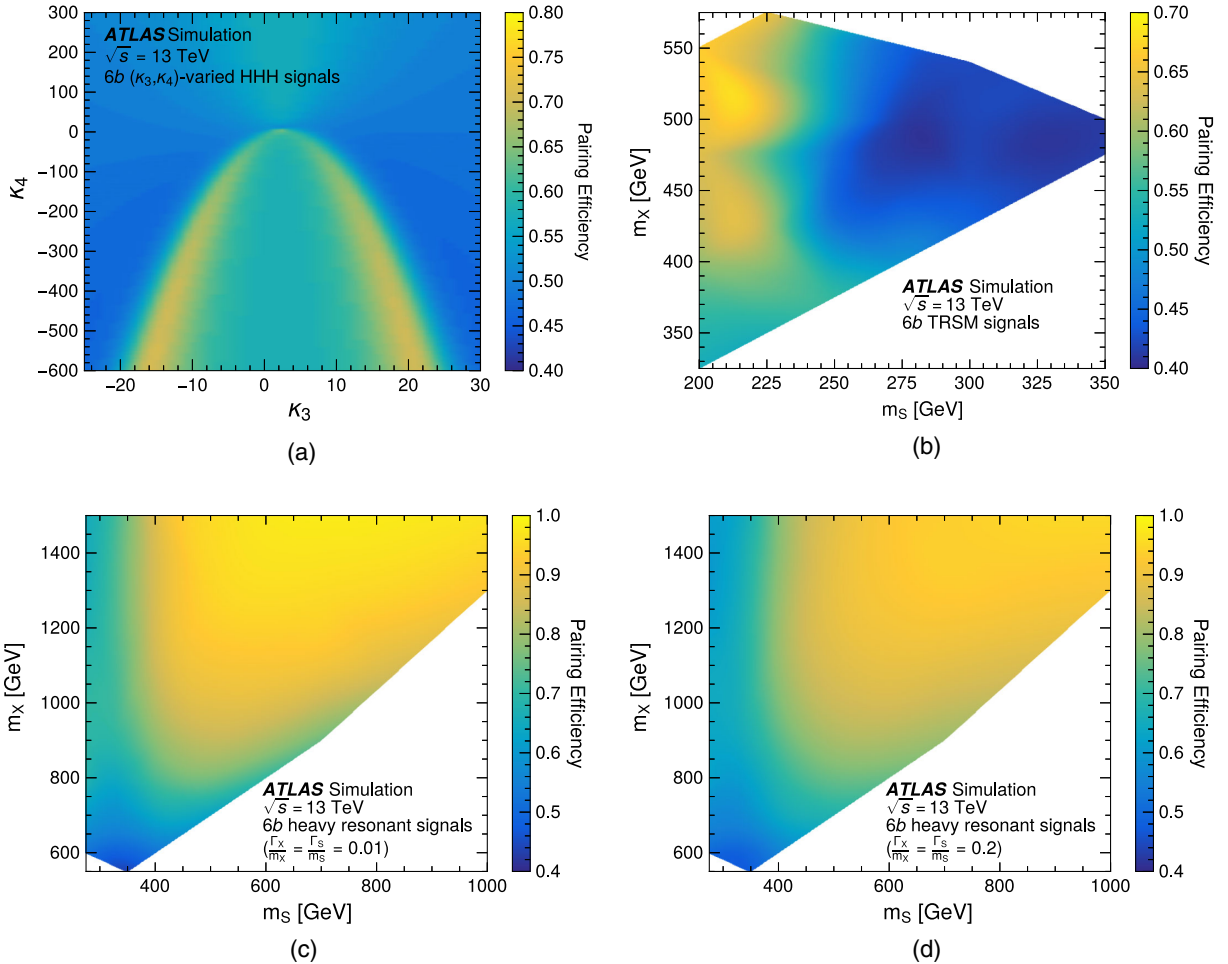

FIG. 3.   Jet pairing efficiencies over the parameter space for the (a) SM-like (κ_3, κ_4) scan, (b) TRSM, and (c) narrow-width or (d) wide-width heavy-resonance signals. The pairing efficiency is evaluated in the $6b$ region when a correct pairing is possible—that is, the six leading jets are geometrically matched to truth-level b-quarks. A cubic Bézier polynomial is used to interpolate across the plane. Areas of the (m_X, m_S) phase space not covered by this search are shown in white.

pairing. For the SM-like and TRSM planes, the kinematic changes are due to the changes in interference between diagrams across the parameter space.

C. Machine learning classifiers

A DNN is trained to classify events as signal- or background-like for each search: nonresonant (nonresDNN), resonant (resDNN), and heavy resonant (heavyresDNN). The resulting classifier score distribution for each search is used as the final analysis discriminant.

For all DNNs, data events in the $5b$ region (which form the basis of the background estimation, as is discussed in Sec. VI) are used as the background training sample. Potential signal contamination in $5b$ data is considered to have a negligible impact for this purpose, as it has yields of $O(1\%)$ of the $5b$ data yield, depending on the signal model. All resonant TRSM signals are combined to form the resDNN signal training sample, and all heavy-resonance signals (both narrow and wide width) are combined to form the heavyresDNN signal training sample. Each simulated (m_X, m_S) point is equally weighted in the training samples. For nonresDNN, the SM HHH signal, which has similar kinematics to the nonresonant TRSM signals, is used as the signal training sample.

These signals were chosen to maximize the training sample size and to group samples with similar enough kinematics for the DNN to perform well. The performance is enhanced by assigning "class weights" to the background, such that the effective yield matches the signal yields during training. To avoid overtraining and benefit from the full set of available events, orthogonal training and testing/validation datasets are used, through a k-fold splitting procedure with $k = 2$ [56], split by odd vs even event numbers. Two DNNs are trained such that the network trained on one half of the events is applied to the other half of the events in the analysis.

For each DNN, ten discriminating kinematic variables are chosen as input features. The ten variables are chosen from a larger set of kinematic variables that have good shape separation between signals and backgrounds. The ten chosen features have the highest Shapley values [57] (a common measure to quantify how impactful an input feature is on the classifier output) and minimize absolute correlations between variables to reduce redundancy. Variables that are correlated differently in signal and background samples are *not* excluded, as they provide discriminating power. In addition, variables are chosen to have minimal correlation with the b-jet multiplicity to

TABLE I.   Summary of the input variables used in each DNN. Check marks denote which input is used for each DNN.

Variable	Definition	Nonres	Res	Heavyres
m_H-radius	Distance between the event (m_{H1}, m_{H2}, m_{H3}) vector and expected vector for signal events, $(120, 115, 110)$GeV.	✓		✓
m_{H1}	Reconstructed mass of the highest p_T Higgs boson candidate.	✓		✓
RMS(m_{jj})	Root-mean-squared (RMS) of the invariant mass of all 15 possible jet pairs.	✓		✓
RMS(ΔR_{jj})	RMS of the angular separation between all 15 possible jet pairs.	✓	✓	✓
RMS(η)	RMS of the pseudorapidity of the Higgs boson candidates.	✓		✓
Skewness ΔA_{jj}	Skewness of $\cosh(\Delta\eta_{ik}) - \cos(\Delta\phi_{ik})$, where i, k are all 15 possible jet pairs.		✓	
H_T^{6j}	Scalar sum of the p_T of the 6 jets selected to reconstruct the 3 Higgs boson candidates.		✓	
$\cos\theta$	In the (m_{H1}, m_{H2}, m_{H3}) coordinate system, θ is the angle between the vector from the origin to the event's reconstructed mass of the Higgs boson candidates, and the vector from the origin to $(120, 115, 110)$GeV.		✓	
Aplanarity$_{6j}$	The fraction of p_T from the 6 jets selected lying outside the plane formed by the 2 highest p_T jets [58].	✓	✓	✓
Sphericity$_{6j}$	Isotropy of the momenta of the 6 jets selected to reconstruct the 3 Higgs boson candidates [58].		✓	
Transverse Sphericity$_{6j}$	Isotropy of the p_T of the 6 jets used for Higgs reconstruction, within the $x - y$ plane [58].	✓		
Sphericity	Isotropy of the momenta of all jets in the event [58].			✓
$\eta - m_{HHH}$ fraction	$\frac{\sum_{i,k} 2p_T^i * p_T^k *(\cosh(\Delta\eta(ik))-1)}{m_{HHH}^2}$, where i, k are all 15 possible jet pairs, and m_{HHH} is the reconstructed tri-Higgs invariant mass.		✓	
ΔR_{H1}	Angular separation between the jets paired to form the highest p_T Higgs boson candidate.	✓	✓	✓
ΔR_{H2}	Angular separation between the jets paired to form the second-highest p_T Higgs boson candidate.	✓	✓	✓
ΔR_{H3}	Angular separation between the jets paired to form the lowest p_T Higgs boson candidate.	✓	✓	✓

reduce the size of the systematic uncertainties in the *b*-jet multiplicity extrapolation.

The input features for each DNN are listed and defined in Table I. Aplanarity and sphericity variables capture differences in the global event shape and are described further in Ref. [58]. Nonresonant and low-mass-resonant *HHH* tend to produce more isotropically distributed jets, while higher mass *X* resonances tend to produce more planar events. The distributions of the most powerful kinematic variable for each DNN are shown in Fig. 4. Distributions for 4*b*, 5*b*, and 6*b* data and example signal

samples are shown. Ratios of data with different *b*-jet multiplicities, including the double ratio (ratio 6*b*/5*b* over ratio 5*b*/4*b*) are additionally shown. The double ratio is used to estimate the background modeling systematic uncertainties, as described in Sec. VIII.

The DNNs are implemented using Keras [59] with a Tensorflow [60] backend. A standard binary cross-entropy loss function is used, with rectified linear unit (ReLU) activation [61,62], an Adam [63] optimizer, and dropout regularization [64] between layers. The hyperparameters were optimized to maximize the sensitivity of the analysis.
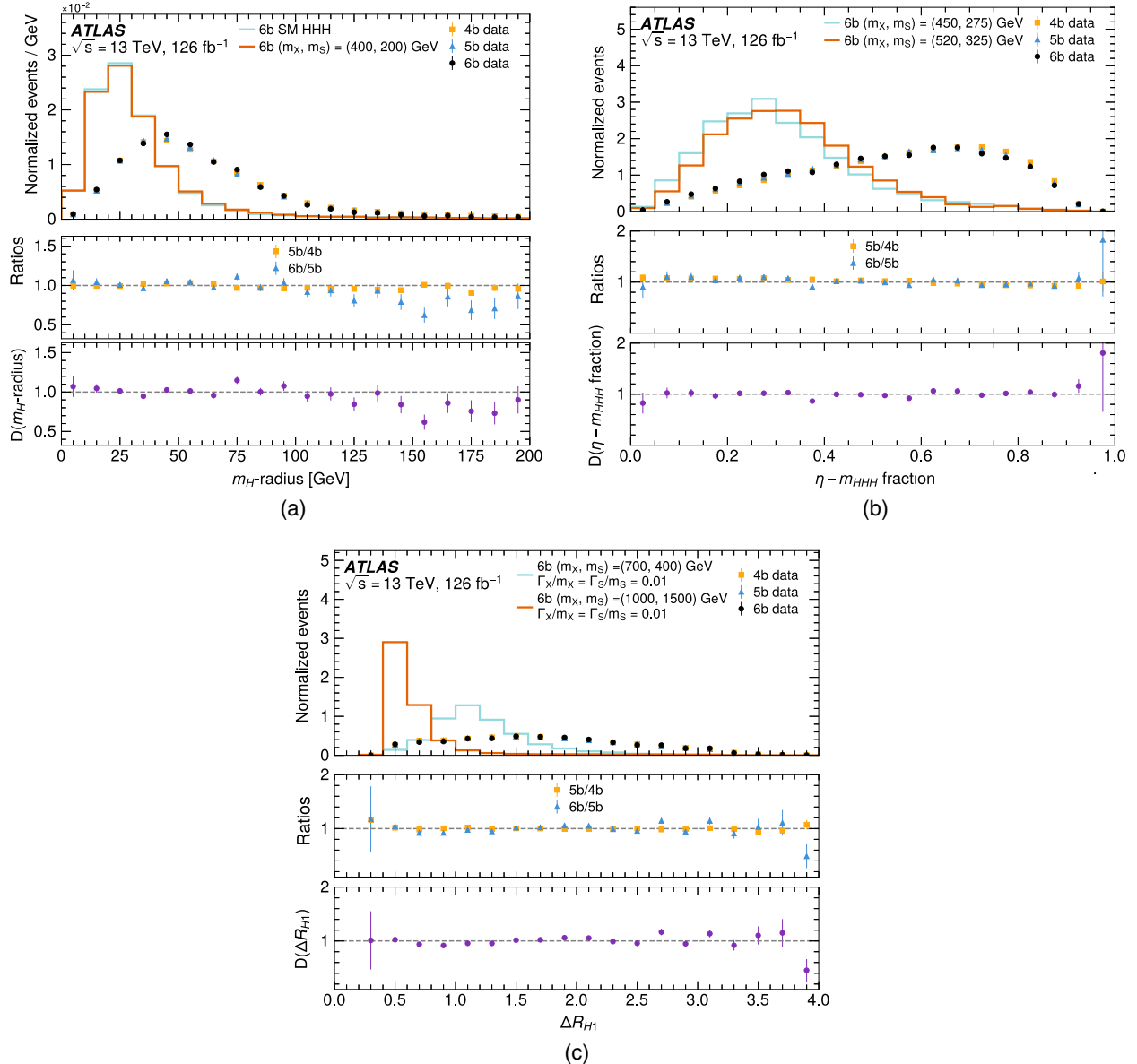

FIG. 4. In the top panel of each plot, the distribution of the most discriminating variable used in each DNN training is shown: (a) m_H radius for nonresDNN, (b) $\eta - m_{HHH}$ fraction for resDNN, and (c) ΔR_{H1} for heavyresDNN. The distributions for the 4*b*, 5*b*, and 6*b* data and example signal samples are shown, with all histograms normalized to unit area. In the middle panel of each plot, the ratios of data with different *b*-jet multiplicities are shown. Finally, in the bottom panel, the ratio 6*b*/5*b* divided by the ratio 5*b*/4*b*—*D*—is shown for data. *D* is used to estimate the size of the systematic uncertainty in the *b*-jet extrapolation method, as described in Sec. VIII.

These include three hidden layers with 24 hidden nodes per layer, a learning rate of 0.01 (0.005), a batch size of 128 (256), and a dropout rate of 0.1, for resDNN (nonresDNN). For heavyresDNN, this includes four hidden layers with 24 hidden nodes per layer, a learning rate of 0.005, a batch size of 256, and a dropout rate of 0.1.

All DNN score distributions span from zero to one. For nonresDNN, the low-score region starts above 0.100 (defined such that below this value the background DNN score distribution extrapolation fails to model the observed 6b data within 1 standard deviation), and the high-score region (containing 90% of the combined signal yield) above 0.552. For resDNN, the low-score region starts above 0.05, and the high-score region above 0.367. For heavyresDNN, the low-score region starts above 0.100, and the high-score region above 0.790.

VI. BACKGROUND ESTIMATION

As introduced in Sec. V, the dominant background process for a final state of ≥ 6 b-quarks is QCD multijet production. The background is modeled via a data-driven approach using the data with four and five b-jets to predict the background yields with at least six b-jets. The assumption of this method is that the kinematic properties of the background do not significantly change relative to b-jet multiplicity, as is observed in Fig. 4 for the most important kinematic features used in the DNNs. The assumption is further validated by comparing the ratio of 4b and 5b data evaluated exclusively in the low- and high-score regions. Therefore, background-enriched regions in the DNN score and b-jet multiplicity are used to construct the 6b background model and its associated systematic uncertainties in the search region. The feature selection strategy (described in Sec. V C) minimizes the difference between the shape of the DNN score distribution in 4b and 5b data and, therefore, reduces the size of the associated uncertainties, which are discussed in Sec. VIII.

Both the low- and high-score regions for 5b and 6b data are included in the fit, as discussed in Sec. V. The low-score region is used to estimate the background shape uncertainties, as discussed in Sec. VIII. The excluded region tends to have large shape differences between 4b, 5b, and 6b data and is not used for the remainder of the analysis. The removal of the excluded region is crucial to ensure that the analysis operates in a region where the kinematic

properties are not highly dependent on b-jet multiplicity, reducing the size of the systematic uncertainties and ensuring that by construction, the assumptions of the method remain valid in the low- and high-score regions.

Data in the 4b and 5b low- and high-score regions are used to model the expected background contribution in the 6b low- and high-score regions, respectively. For each DNN, an extrapolation across b-jet multiplicities is performed in the DNN score to model the expected background contribution in the 6b region,

$$N_i^{6b,\text{predicted}} = \mu_{\text{NF}} \cdot B_i \cdot \left(\frac{(N^{5b}/N^{4b})_i}{N^{5b}/N^{4b}} \right), \qquad (2)$$

where N is the observed number of events (except when explicitly noted, as in $N_i^{6b,\text{predicted}}$), B are a set of unconstrained bin-by-bin parameters fit from the 5b region, the superscript denotes the region (4b, 5b, or 6b), and the subscript i denotes the i-th bin in the DNN score distribution. The normalization on the background model is μ_{NF}, which is fit *in situ* to the data, as described in the next section. In the case where there is no signal contribution, $\mu_{\text{NF}} = N^{6b}/N^{5b}$ and $B_i = N_i^{5b}$. However, when the signal strength is nonzero, $\mu_{\text{NF}} < N^{6b}/N^{5b}$ and $B_i < N_i^{5b}$.

The inclusion of the term $(N^{5b}/N^{4b})_i/(N^{5b}/N^{4b})$ in Eq. (2) extrapolates the shape of the DNN score distribution as a function of b-jet multiplicity. Such a shape extrapolation is observed to produce better modeling in the low-score region.

VII. STATISTICAL INTERPRETATION

Test statistics are built from the profile likelihood ratio (PLR) following the prescription for discovery of a positive signal and one-sided upper limits detailed in Ref. [65]. The likelihood model assumes independent Poisson-distributed event counts in each bin of the 5b and 6b DNN score distributions in the low-score and high-score regions, which are included in the fit. Nuisance parameters (NPs) describing the effect of systematic uncertainties in the signal $(\vec{\phi})$ are fully correlated between the 5b and 6b regions. An orthogonal set of NPs $\vec{\theta}$ describes the background extrapolation from the 5b to the 6b region. The full expression of the parametrized likelihood model of the observed yields is as follows:

$$\mathcal{L}(\vec{N}^{5b,6b}, \vec{S}^{5b,6b} | \vec{\theta}, \vec{\phi}, \vec{\gamma}^{5b,6b}, \mu_{\text{s}}, \mu_{\text{NF}}) = \prod_{i \in \text{bins}} [\text{Pois}(N_i^{6b} | \mu_{\text{NF}} f_i(\vec{\theta}) B_i + \mu_{\text{s}} w_i^{6b}(\vec{\phi}) \gamma_i^{6b} S_i^{6b}) \text{Pois}(N_i^{5b} | B_i + \mu_{\text{s}} w_i^{5b}(\vec{\phi}) \gamma_i^{5b} S_i^{5b})]$$

$$\times \prod_{m \in \text{bkg.systs}} \frac{1}{\sqrt{2\pi}} e^{-\theta_m^2/2} \prod_{k \in \text{sig.systs}} \frac{1}{\sqrt{2\pi}} e^{-\phi_k^2/2}$$

$$\times \prod_{i \in \text{bins}} [P_\Gamma(\nu_i^{5b} | \gamma_i^{5b} \nu_i^{5b}) P_\Gamma(\nu_i^{6b} | \gamma_i^{6b} \nu_i^{6b})]. \qquad (3)$$

The first two Poissonian terms describe the constraints from the observed data $\vec{N}$. Superscripts $5b$ and $6b$ are used throughout to distinguish the $5b$ CR from the $6b$ SR. Signal leakage into the $5b$ region is considered via S_i^{5b}. B_i are an unconstrained set of bin-by-bin yields fit from the CR and μ_s is the signal strength and the parameter of interest (for the limits on the coupling modifiers κ_3 and κ_4, the signal expression is altered, such that κ_3 and κ_4 become two parameters of interest in the fit). The precise manner in which $\vec{\phi}$ and $\vec{\theta}$ change each bin of the yields is encapsulated in $w_i(\vec{\phi})$ and $f_i(\vec{\theta})$, respectively. The nominal value of $f_i(\vec{\theta})$ is the ratio of the DNN score shapes for the $5b$ and $4b$ data, $((N^{5b}/N^{4b})_i)/(N^{5b}/N^{4b})$, as appears in Eq. (2). Therefore, $f_i(\vec{\theta})$ performs the DNN score shape extrapolation to the $6b$ region. The uncertainties in the extrapolation are assessed using alternative shapes, as discussed in Sec. VIII. The nominal value of $w_i(\vec{\phi})$ is unity, and it describes the way theoretical and experimental uncertainties both change the shape and normalization of the signal.

The third and fourth terms (products over m and k) describe the Gaussian constraints for the NPs. The observed MC signal yields $\vec{S}$ are multiplied by nuisance parameters $\vec{\gamma}$ in the final term to account for the limited MC sample size. The generalization of the Poisson distribution to continuous variables P_Γ is used to represent the MC statistical uncertainty by constraining $\vec{\gamma}$. The $\vec{\nu}$ are constants constructed to provide the correct uncertainty sizes in the constraint term; they can be viewed as "effective" numbers of MC events, accounting for event weighting.

The choice of binning is different for each of the three DNNs. The resDNN score distribution is fit from 0.05 to 1.0 in 19 bins of equal width 0.05. The heavyresDNN score distribution is fit from 0.1 to 1.0 with equally spaced bins of 0.05. Likewise, the nonresDNN score is fit in the region 0.1–1.0 with equal bins of width 0.05, except for the final bin, which is subdivided into two equally sized bins of width 0.025. Dividing the final bin in this search increases sensitivity. The choice of binning is a trade-off between sensitivity and the ability to model systematic uncertainties in the data-driven background shape, as discussed in the next section.

VIII. SYSTEMATIC UNCERTAINTIES

The systematic uncertainties considered include experimental uncertainties, uncertainties in the shape of the data-driven background modeling of the DNN score distribution, and theoretical modeling uncertainties in the simulated signal samples.

The dominant systematic uncertainty in this search is the uncertainty in the shape of the background DNN score distribution. As described in Sec. VI, the background model extrapolates the shape of the DNN score distribution as a function of the b-jet multiplicity, with the

normalization of the background model μ_{NF} determined *in situ* by the fit to the observed data. Due to the data-driven nature of the background estimate, the shape extrapolation uncertainty is the only systematic uncertainty that affects the background prediction. The shape extrapolation will agree with the $6b$ data perfectly when the DNN score shape differences between the $6b$ and $5b$ regions agree with the shape differences between $5b$ and $4b$. However, this cannot be assumed, and the size of the nonclosure in the extrapolation method in the signal-depleted low-score region is used to estimate the systematic uncertainty in the extrapolation method. The double ratio $D(v)$ is introduced, which compares the shape differences between the $6b$ and $5b$ regions and the $5b$ and $4b$ regions (each themselves ratios) as a function of the DNN input variable v,

$$D(v) = \left(\frac{(N^{6b}/N^{5b})(v)}{N^{6b}/N^{5b}}\right)_{\text{Low-Score}}$$
$$\div \left(\frac{(N^{5b}/N^{4b})(v)}{N^{5b}/N^{4b}}\right)_{\text{Low-Score}}, \qquad (4)$$

where the ratios in the numerators are functions of the DNN input variable v in the low-score region. The double ratio $D(v)$ is thus the nonclosure in the multiplicative extrapolation method in the low-score region as a function of v. The binned quantity $D_i(v)$ is $D(v)$ averaged over the events in bin i of the DNN score distribution. In this context, i runs over both low- and high-score regions, thereby applying the observed nonclosure in the low-score region as a systematic uncertainty in the high-score region.

Nonclosure in the extrapolation method is quantified by deviations from $D_i(v) = 1$. The nominal background model [Eq. (2)] is reweighted by the value of $D_i(v)$ to produce a set of systematically varied models, with each of the ten DNN inputs producing a different template. The variations are considered fully correlated between each bin i of the DNN. This method does not rely on any assumption that $D_i(v) = 1$. Rather, it assumes that deviations from $D_i(v) = 1$ due to background processes are similar in the low-score and high-score regions. This assumption is validated in the background-enriched $4b$ and $5b$ regions. It is observed that the ratios $(N^{5b}/N^{4b})(v)$ evaluated in the low- and high-score regions are compatible within statistical fluctuations, an agreement which has been reinforced by removing the very-low-score events (excluded region) from the analysis. The multiplicative variations to the nominal background template from $D_i(v)$ are symmetrized about $D_i(v) = 1$ for up and down variations.

Only a subset of ten possible shape variations (one for each of the ten DNN input variables) are applied as systematic uncertainties. A pruning procedure is used that removes shape variations that are expressible as linear combinations of other shape variations to avoid double counting. The pruning procedure is to iteratively add new systematic variations (ordered by largest single bin

deviation) until the set of excluded variations are well modeled by the set of included variations. Specifically, a profile likelihood fit to each of the excluded variations is performed, with the only degrees of freedom being the included shape variations. The procedure terminates once the maximum χ^2 of all of the fits to the excluded shapes is less than 1. It is found that for each DNN, a subset of three shape variations is enough to model all ten shapes sufficiently well.

Figure 5 shows the pruned subset of shape variations for each of the DNNs. The shape variations are always smaller than the statistical uncertainty in the expected $6b$ data. For reference, the $5b$ data without extrapolation are shown. The difference between the observed $5b$ data and the extrapolated nominal $6b$ template is on the same order as the derived shape systematic variations.

Experimental uncertainties in luminosity, pile-up reweighting, jet energy scale and resolution, NNJVT efficiency, trigger efficiency, and b-tagging efficiency are

considered. As the background model is entirely data-driven, these uncertainties only affect the simulated signal MC events. The pile-up uncertainty is estimated according to the methods described in Ref. [66]. Uncertainties in the jet energy scale and resolution, NNJVT efficiency, and b-tagging efficiency are applied on a per-jet level and are estimated from calibrations and comparisons between different event simulation models [40,41,67]. The uncertainty in the NNJVT efficiency is estimated following the technique in Ref. [42].

The uncertainty in the trigger efficiency is estimated in data and MC using triggers requiring one muon and one jet so as not to bias the fully hadronic trigger efficiency measurement. The uncertainty in the jet-level trigger SF is estimated as the difference between the nominal SF and a SF derived using $t\bar{t}$ MC samples with different matrix elements and parton shower models. One alternative sample uses an alternative matrix element NLO matching scale (pThard), and another uses HERWIG7 [68] in place of
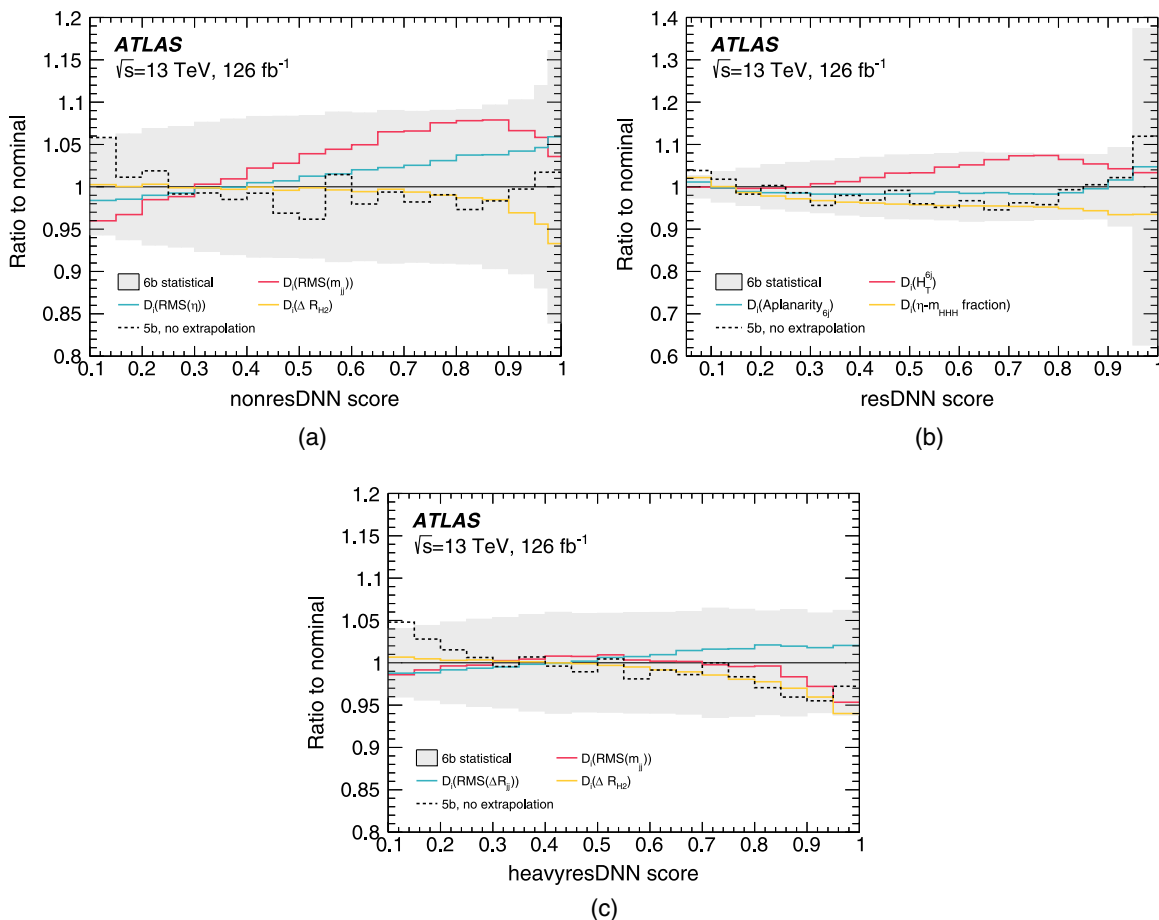

FIG. 5.   Ratios of the shape-varied models relative to the nominal background models $[D_i(v)]$ for the selected input kinematics that survived pruning of the (a) nonresDNN, (b) resDNN, and (c) heavyresDNN. The gray band is the size of the statistical uncertainty in the expected $6b$ background for reference. The dashed line is the shape of the $5b$ data with no extrapolation applied. The shape systematic uncertainties are all smaller than the expected $6b$ background statistical uncertainty for each bin and are on the same order as the size of the extrapolation from $5b$ data. The binning matches exactly the scheme used for the PLR fit, as described in Sec. VII.

Pythia8 for the parton showering. The event-level SF applied is built from the jet-level SFs considering all possible combinations of which jets may have fired the trigger.

A 5% uncertainty is applied to the signal MC samples to cover the differences between the *b*-tagging applied at trigger level (MV2c10 for 2016 and MV2c20 for 2017–2018) [20] and at reconstruction level (DL1d) [43–45]. Given that an event has satisfied the offline selection of six *b*-jets, it has a larger than 99% chance of satisfying the trigger's online *b*-tagging. Therefore, the 5% uncertainty is much larger than the trigger inefficiency in the region most sensitive to the presence of a signal.

Modeling uncertainties in the signal MC event simulations are also considered and are calculated using an identical procedure for all signal models considered. To estimate the uncertainty due to higher-order terms in the perturbative expansion of the cross section, a 7-point variation in renormalization and factorization scales is used. Both scales are either kept at their nominal values or varied independently up and down by a factor of 2 and 0.5, while the schemes in which one scale is varied up and the other is varied down are excluded for a total of seven possible choices of renormalization and factorization scales. The uncertainty applied to the signal MC is an envelope around the seven variations. An alternative value of the strong coupling constant α_S is also used, and the difference is taken as an uncertainty. A systematic uncertainty in the choice of PDF is applied as the standard deviation of 100 variations in the NNPDF3.0NLO PDF set.

Table II summarizes the impact of each set of systematic uncertainties in the expected upper limit. Each row shows the difference between the upper limit with all sources of uncertainty considered and the upper limit with a subset of the systematic uncertainties excluded. Each cell shows the range of impacts for the various mass hypotheses m_X and

m_S considered for each of the three DNNs. The systematic uncertainties in the background shape are the dominant sources of systematic uncertainty, changing the expected limit by 14% to 45% depending on the model and BSM masses m_X and m_S. Flavor tagging, jet reconstruction, and trigger efficiency uncertainties are the subleading sources of systematic uncertainty, with an impact of up to 10% on the expected upper limit.

IX. RESULTS

The distributions of the nonResDNN, resDNN, and heavyResDNN scores in the $6b$ region after the profile likelihood fit described in Sec. VII can be found in Fig. 6. One representative signal point is overlaid on each score distribution, scaled to the same area as the background distribution. For nonresDNN, the SM *HHH* signal and a nonresonant TRSM signal with $(m_X, m_S) = (400, 200)$ GeV are both shown in Figs. 6(a) and 6(b), respectively. In all cases, the observed data agree well with the background, and no significant excess is seen. For the resonant search, no upward deviation from the SM prediction is observed. A one-sided test statistic is used, and the best-fit signal is precisely zero for all mass points considered. For the nonresonant search, the largest deviation is at $(m_X, m_S) = (550, 200)$ GeV with a local significance of 0.19σ. For the heavy-resonant search, the largest deviation is at $(m_X, m_S) = (1500, 275)$ GeV with a local significance of 0.51σ.

Upper limits for each signal model considered are placed on the allowed *HHH* production cross section, at the 95% CL. They are calculated using the CL_s method [69] with the asymptotic approximation [65].

For the TRSM and DM-CPV models, expected and observed cross section upper limits are shown over the

TABLE II. Summary of the impact on the analysis of different sources of systematic uncertainty. The impact is estimated as the absolute value of the difference between the expected upper limit with all sources of uncertainty included and the upper limit with a subset of systematic uncertainties excluded. In the left-hand column, more heavily indented rows are a subcategory of the less indented row above.

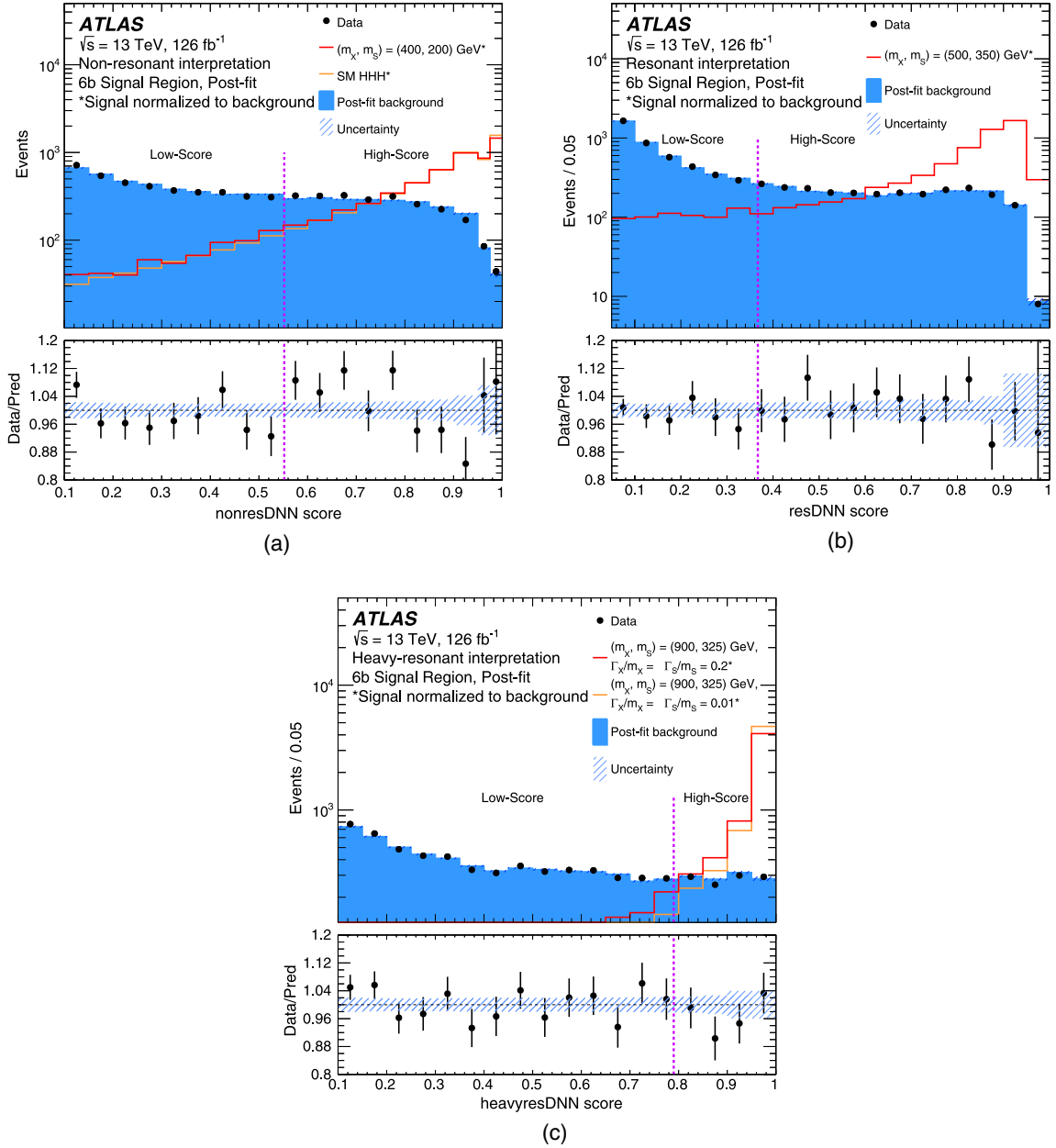| Uncertainty source	Relative impact of systematic uncertainties (%)			
	SM-like	TRSM nonresonant	TRSM resonant	Heavy resonance
All uncertainties	24	20–46	33–42	24–53
Experimental	22	20–45	33–41	24–53
Detector response	7.4	6.6–14	16–24	4.1–15
Luminosity and pile-up	<1	<1	<1	<1
Flavor tagging	3.2	2.8–5	6.9–8.8	1.5–5.6
Jet reconstruction	2.7	2.3–6.5	3.6–7.1	1.0–6.3
Trigger efficiency	2.0	1.8–3.5	6–10	1.4–4.2
Background modeling	16	14–36	18–30	20–45
Theoretical	1.5	<1	<1	<1
MC statistical	<1	<1	<1	<1

FIG. 6. Distributions of scores for (a) nonresDNN, (b) resDNN, and (c) heavyresDNN in 6*b* data and the background prediction after background-only fits to the observed data. The boundary between the low- and high-score regions is shown by a dashed vertical line. Benchmark signal models (normalized to the background) are overlaid in each case: (a) SM *HHH* signal and nonresonant TRSM signal with $(m_X, m_S) = (400, 200)$ GeV, (b) resonant TRSM signal with $(m_X, m_S) = (500, 350)$ GeV overlaid, and (c) narrow- and large-width heavy resonances with $(m_X, m_S) = (900, 325)$ GeV overlaid. The lower panel in each plot shows the ratio of the data and the post-fit background (Pred) in markers, with the uncertainty on the prediction shown as a hatched band centered on unity.

(m_X, m_S) plane in Figs. 7(a) and 7(b), respectively. The $m_S > 250$ GeV region forms the resonant search, where resDNN is used in the fit, whereas the $m_S < 250$ GeV region is part of the nonresonant search, where nonresDNN is used in the fit. The expected (observed) cross section upper limit varies with m_X and m_S, within the range of 46–350 fb (48–310 fb). The limits are evaluated at the simulated (m_X, m_S) points, as described in Sec. III. For all results in the analysis, a cubic Bézier polynomial is used to interpolate across the plane.

The cross section upper limits for the heavy-resonance search are shown in Fig. 8 in the (m_X, m_S) plane. Expected (observed) limits for the narrow heavy-resonance signals are presented in Fig. 8(a) [Fig. 8(c)], and range between 4.7 and 69 fb (5.7 and 38 fb). Expected (observed) limits for the wide heavy-resonance signals are presented in Fig. 8(b) [Fig. 8(d)], and range between 5.2 and 53 fb (6.3 and 39 fb).

Simultaneous limits on the coupling modifiers κ_3 and κ_4 are shown in Fig. 9. The gray dashed line shows the region
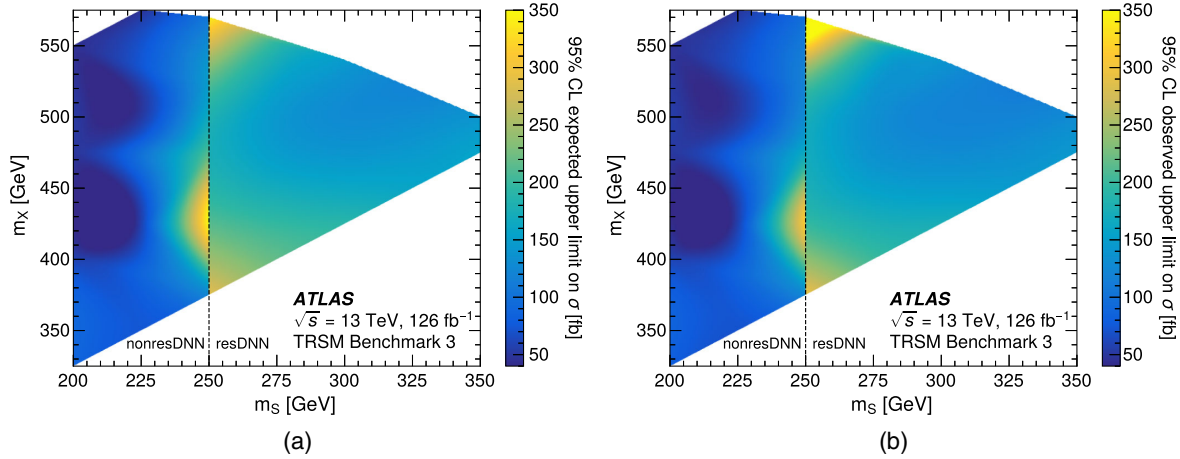
FIG. 7. (a) Expected and (b) observed 95% CL *HHH* cross section upper limits for the phase space within the perturbative unitarity bounds of the TRSM. While the points were generated under benchmark point 3 of the TRSM, they can also be interpreted in the DM-CPV model. The white areas correspond to regions of the (m_X, m_S) phase space not considered here. A cubic Bézier polynomial is used to interpolate across the plane.
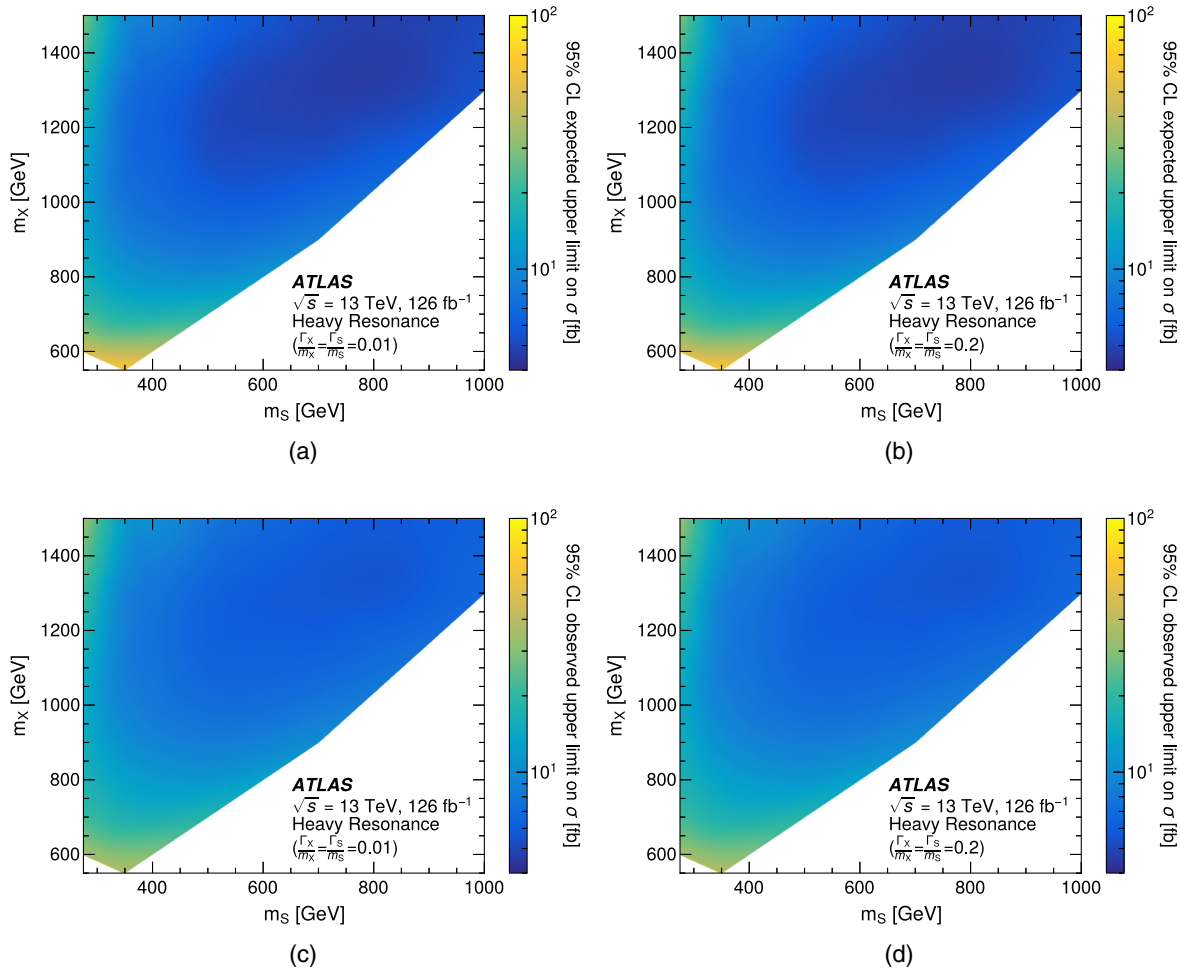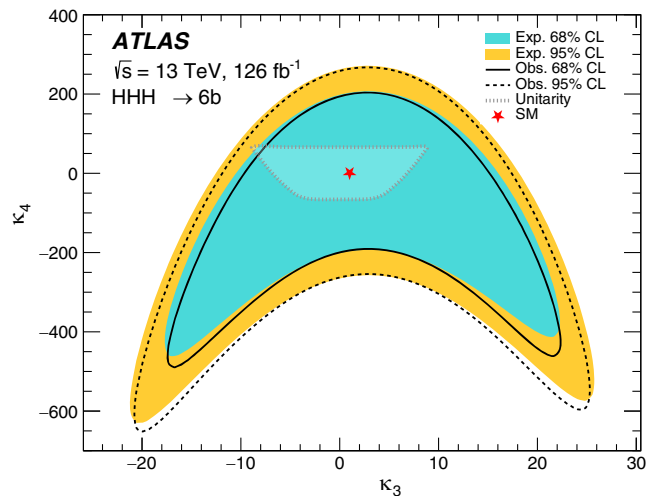

FIG. 8. (a), (b) Expected and (c), (d) observed 95% CL *HHH* cross section upper limits for the (a), (c) narrow-width or (b), (d) wide-width heavy-resonance signals. The white areas correspond to regions of the (m_X, m_S) phase space not considered here. A cubic Bézier polynomial is used to interpolate across the plane.

FIG. 9. Expected (filled regions) and observed (black solid and dashed lines) 95% and 68% CL constraints on κ_3 and κ_4, the ratios of the Higgs trilinear and quartic self-couplings to their predicted SM values. Unitarity limits, calculated in Ref. [70], are overlaid in the region bounded by the gray dashed line. The red star is the SM: $\kappa_3 = \kappa_4 = 1$.

where perturbative unitarity holds (provided that κ_3 and κ_4 are the only modifications to the SM), as calculated in Ref. [70]. At the 95% CL, none of the phase space inside the unitarity bounds is excluded. Outside the unitarity bounds, the kappa framework requires additional modification to preserve unitarity, and as such it is not recommended to interpret this result as excluding any relevant phase space in the kappa framework. Rather, the scan of κ_3 and κ_4 serves as a benchmark of performance for future searches and projections, as well as other new-physics models, which may produce similar phenomenology.

The observed (expected) 95% CL upper limit on the signal strength for SM HHH production, $\mu = \sigma_{HHH}/\sigma_{HHH}^{SM}$, is 760 (750), corresponding to an observed cross section upper limit of 59 fb (59 fb). Assuming $\kappa_4 = 1$, then κ_3 is restricted to be between -11 and 17 at the 95% CL (both for expected and observed limits). For comparison, a combination of previous di-Higgs searches and single Higgs production constraints limited κ_3 to be between -0.4 and 6.3 at 95% CL [7]. Assuming $\kappa_3 = 1$, then κ_4 is restricted to be between -230 and 240 at the 95% CL (both for expected and observed limits).

X. CONCLUSION

This paper presented a search for triple Higgs production in the $b\bar{b}b\bar{b}b\bar{b}$ final state. The search used 126 fb^{-1} of pp collision data at $\sqrt{s} = 13$ TeV collected with the ATLAS detector at the LHC. The data were interpreted using three different DNNs, which were each optimized to search for nonresonant, resonant, and heavy-resonant (outside the perturbative unitarity bounds of the TRSM) signals with additional scalars. The nonresonant interpretation included a

search for SM-like signals with coupling modifiers on the trilinear and quartic Higgs self-couplings κ_3 and κ_4. The SM background was modeled using a data-driven extrapolation method, derived from the observed DNN score spectra in events with four or five b-jets to estimate the background shape in events with at least six b-jets. The sensitivity of the search was impacted mainly by the statistical precision and the uncertainty in the data-driven extrapolation method.

No significant excess above the SM expectation was observed in the search for SM HHH production, nor was any significant excess observed in the search for various BSM signals with two additional heavy scalars, X and S. A 95% CL upper limit of 59 fb was set on the cross section for SM HHH production. The BSM searches included non-resonant production, where $m_S < 250$ GeV, and resonant production up to $(m_X, m_S) = (1500, 1000)$ GeV.

DATA AVAILABILITY

The data that support the findings of this article are not publicly available. The values in the plots and tables associated to this article are stored in HEPDATA [72].

---

[1] ATLAS Collaboration, Observation of a new particle in the search for the standard model Higgs boson with the ATLAS detector at the LHC, Phys. Lett. B **716**, 1 (2012).

[2] CMS Collaboration, Observation of a new boson at a mass of 125 GeV with the CMS experiment at the LHC, Phys. Lett. B **716**, 30 (2012).

[3] ATLAS Collaboration, A detailed map of Higgs boson interactions by the ATLAS experiment ten years after the discovery, Nature (London) **607**, 52 (2022).

[4] CMS Collaboration, A portrait of the Higgs boson by the CMS experiment ten years after the discovery, Nature (London) **607**, 60 (2022).

[5] LHC Higgs Cross Section Working Group, LHC HXSWG interim recommendations to explore the coupling structure of a Higgs-like particle, arXiv:1209.0040.

[6] ATLAS Collaboration, Combination of searches for Higgs boson pair production in pp collisions at $\sqrt{s} = 13$ TeV with the ATLAS detector, Phys. Rev. Lett. **133**, 101801 (2024).

[7] ATLAS Collaboration, Constraints on the Higgs boson self-coupling from single- and double-Higgs production with the ATLAS detector using pp collisions at $\sqrt{s} = 13$ TeV, Phys. Lett. B **843**, 137745 (2023).

[8] A. Papaefstathiou, G. Tetlalmatzi-Xolocotzi, and M. Zaro, Triple Higgs boson production to six b-jets at a 100 TeV

proton collider: Anomalous self-couplings and gauge-singlet scalars, Eur. Phys. J. C **79,** 947 (2019),

[9] A. Papaefstathiou and G. Tetlalmatzi-Xolocotzi, Multi-Higgs boson production with anomalous interactions at current and future proton colliders, J. High Energy Phys. 06 (2024) 124.

[10] H. Abouabid *et al.*, HHH whitepaper, Eur. Phys. J. C **84,** 1183 (2024).

[11] ATLAS Collaboration, The ATLAS experiment at the CERN large hadron collider, J. Instrum. **3,** S08003 (2008).

[12] A. Papaefstathiou, T. Robens, and G. Tetlalmatzi-Xolocotzi, Triple Higgs boson production at the large hadron collider with two real singlet scalars, J. High Energy Phys. 05 (2021) 193.

[13] T. Robens, T. Stefaniak, and J. Wittbrodt, Two-real-scalar-singlet extension of the SM: LHC phenomenology and benchmark scenarios, Eur. Phys. J. C **80,** 151 (2020).

[14] T.-K. Chen, C.-W. Chiang, and I. Low, A simple model of dark matter and *CP* violation, Phys. Rev. D **05,** 105 (2022).

[15] G. Avoni *et al.*, The new LUCID-2 detector for luminosity measurement and monitoring in ATLAS, J. Instrum. **13,** P07017 (2018).

[16] ATLAS Collaboration, Performance of the ATLAS trigger system in 2015, Eur. Phys. J. C **77,** 317 (2017).

[17] ATLAS Collaboration, Software and computing for Run 3 of the ATLAS experiment at the LHC, arXiv:2404.06335.

[18] ATLAS Collaboration, Luminosity determination in pp collisions at $\sqrt{s} = 13$ TeV using the ATLAS detector at the LHC, Eur. Phys. J. C **83,** 982 (2023).

[19] ATLAS Collaboration, ATLAS data quality operations and performance for 2015-2018 data-taking, J. Instrum. **15,** P04003 (2020).

[20] ATLAS Collaboration, Configuration and performance of the ATLAS b-jet triggers in Run 2, Eur. Phys. J. C **81,** 1087 (2021).

[21] M. Cacciari, G. P. Salam, and G. Soyez, The anti-k_t jet clustering algorithm, J. High Energy Phys. 04 (2008) 063.

[22] M. Cacciari, G. P. Salam, and G. Soyez, FastJet user manual, Eur. Phys. J. C **72,** 1896 (2012).

[23] J. Alwall, M. Herquet, F. Maltoni, O. Mattelaer, and T. Stelzer, MadGraph 5: Going beyond, J. High Energy Phys. 06 (2011) 128.

[24] R. D. Ball *et al.* (NNPDF Collaboration), Parton distributions for the LHC run II, J. High Energy Phys. 04 (2015) 040.

[25] ATLAS Collaboration, ATLAS Pythia 8 tunes to 7 TeV data, Report No. ATL-PHYS-PUB-2014-021, 2014, https://cds.cern.ch/record/1966419.

[26] D. de Florian *et al.*, Handbook of LHC Higgs cross sections: 4. Deciphering the nature of the Higgs sector, arXiv:1610.07922.

[27] T. Sjöstrand, S. Ask, J. R. Christiansen, R. Corke, N. Desai, P. Ilten, S. Mrenna, S. Prestel, C. O. Rasmussen, and P. Z. Skands, An introduction to Pythia 8.2, Comput. Phys. Commun. **191,** 159 (2015).

[28] O. Mattelaer, On the maximal use of Monte Carlo samples: Re-weighting events at NLO accuracy, Eur. Phys. J. C **76,** 674 (2016).

[29] A. Papaefstathiou and K. Sakurai, Triple Higgs boson production at a 100 TeV proton-proton collider, J. High Energy Phys. 02 (2016) 006.

[30] D. de Florian, I. Fabre, and J. Mazzitelli, Triple Higgs production at hadron colliders at NNLO in QCD, J. High Energy Phys. 03 (2020) 155.

[31] O. Karkout, A. Papaefstathiou, M. Postma, G. Tetlalmatzi-Xolocotzi, J. van de Vis, and T. d. Pree, Triple Higgs boson production and electroweak phase transition in the two-real-singlet model, J. High Energy Phys. 11 (2024) 077.

[32] P. Artoisenet, R. Frederix, O. Mattelaer, and R. Rietkerk, Automatic spin-entangled decays of heavy resonances in Monte Carlo simulations, J. High Energy Phys. 03 (2013) 015.

[33] ATLAS Collaboration, The ATLAS simulation infrastructure, Eur. Phys. J. C **70,** 823 (2010).

[34] ATLAS Collaboration, AtlFast3: The next generation of fast simulation in ATLAS, Comput. Software Big Sci. **6,** 7 (2022).

[35] S. Agostinelli *et al.*, Geant4—a simulation toolkit, Nucl. Instrum. Methods Phys. Res., Sect. A **506,** 250 (2003).

[36] T. Sjöstrand, S. Mrenna, and P. Skands, A brief introduction to Pythia 8.1, Comput. Phys. Commun. **178,** 852 (2008).

[37] R. D. Ball *et al.* (NNPDF Collaboration), Parton distributions with LHC data, Nucl. Phys. **B867,** 244 (2013).

[38] ATLAS Collaboration, The Pythia 8 A3 tune description of ATLAS minimum bias and inelastic measurements incorporating the Donnachie–Landshoff diffractive model, Report No. ATL-PHYS-PUB-2016-017, 2016, https://cds.cern.ch/record/2206965.

[39] ATLAS Collaboration, Reconstruction of primary vertices at the ATLAS experiment in Run 1 proton–proton collisions at the LHC, Eur. Phys. J. C **77,** 332 (2017).

[40] ATLAS Collaboration, Jet reconstruction and performance using particle flow with the ATLAS Detector, Eur. Phys. J. C **77,** 466 (2017).

[41] ATLAS Collaboration, Jet energy scale and resolution measured in proton–proton collisions at $\sqrt{s} = 13$ TeV with the ATLAS detector, Eur. Phys. J. C **81,** 689 (2021).

[42] ATLAS Collaboration, Performance of pile-up mitigation techniques for jets in pp collisions at $\sqrt{s} = 8$ TeV using the ATLAS detector, Eur. Phys. J. C **76,** 581 (2016).

[43] ATLAS Collaboration, Neural network jet flavour tagging with the upgraded ATLAS inner tracker detector at the high-luminosity LHC, Report No. ATL-PHYS-PUB-2022-047, 2022, https://cds.cern.ch/record/2839913.

[44] ATLAS Collaboration, Deep sets based neural networks for impact parameter flavour tagging in ATLAS, Report No. ATL-PHYS-PUB-2020-014, 2020, https://cds.cern.ch/record/2718948.

[45] ATLAS Collaboration, ATLAS flavour-tagging algorithms for the LHC Run 2 pp collision dataset, Eur. Phys. J. C **83,** 681 (2023).

[46] ATLAS Collaboration, ATLAS b-jet identification performance and efficiency measurement with $t\bar{t}$ events in pp collisions at $\sqrt{s} = 13$ TeV, Eur. Phys. J. C **79,** 970 (2019).

[47] ATLAS Collaboration, Measurement of b-tagging efficiency of c-jets in $t\bar{t}$ events using a likelihood approach

with the ATLAS detector, Report No. ATLAS-CONF-2018-001, 2018, https://cds.cern.ch/record/2306649.

[48] ATLAS Collaboration, Calibration of light-flavour *b*-jet mistagging rates using ATLAS proton–proton collision data at $\sqrt{s} = 13$ TeV, Report No. ATLAS-CONF-2018-006, 2018, https://cds.cern.ch/record/2314418.

[49] ATLAS Collaboration, Evidence for the $H \to b\bar{b}$ decay with the ATLAS detector, J. High Energy Phys. 12 (2017) 024.

[50] ATLAS Collaboration, Muon reconstruction and identification efficiency in ATLAS using the full Run 2 *pp* collision data set at $\sqrt{s} = 13$ TeV, Eur. Phys. J. C **81**, 578 (2021).

[51] ATLAS Collaboration, Muon reconstruction performance of the ATLAS detector in proton–proton collision data at $\sqrt{s} = 13$ TeV, Eur. Phys. J. C **76**, 292 (2016).

[52] S. Frixione, G. Ridolfi, and P. Nason, A positive-weight next-to-leading-order Monte Carlo for heavy flavour hadroproduction, J. High Energy Phys. 09 (2007) 126.

[53] P. Nason, A new method for combining NLO QCD with shower Monte Carlo algorithms, J. High Energy Phys. 11 (2004) 040.

[54] S. Frixione, P. Nason, and C. Oleari, Matching NLO QCD computations with parton shower simulations: The POWHEG method, J. High Energy Phys. 11 (2007) 070.

[55] S. Alioli, P. Nason, C. Oleari, and E. Re, A general framework for implementing NLO calculations in shower Monte Carlo programs: The POWHEG BOX, J. High Energy Phys. 06 (2010) 043.

[56] M. Stone, Cross-validatory choice and assessment of statistical predictions, J. R. Stat. Soc. Ser. B Stat. Method. **36**, 111 (1974).

[57] B. Rozemberczki *et al.*, The Shapley value in machine learning, arXiv:2202.05594.

[58] ATLAS Collaboration, Measurement of event shapes at large momentum transfer with the ATLAS detector in *pp* collisions at $\sqrt{s} = 7$ TeV, Eur. Phys. J. C **72**, 2211 (2012).

[59] F. Chollet *et al.*, Keras, 2015, https://keras.io.

[60] Martín Abadi *et al.*, TensorFlow: Large-Scale Machine Learning on Heterogeneous Systems, Software available from tensorflow.org, 2015, https://www.tensorflow.org/.

[61] K. Fukushima, Visual feature extraction by a multilayered network of analog threshold elements, IEEE Trans. Syst. Sci. Cybern. **5**, 322 (1969).

[62] V. Nair and G. E. Hinton, Rectified linear units improve restricted boltzmann machines, in *Proceedings of the 27th International Conference on International Conference on Machine Learning, ICML'10* (Omnipress, Haifa, Israel, 2010), p. 807, ISBN: 9781605589077.

[63] D. P. Kingma and J. Ba, Adam: A method for stochastic optimization, arXiv:1412.6980.

[64] N. Srivastava, G. Hinton, A. Krizhevsky, I. Sutskever, and R. Salakhutdinov, Dropout: A simple way to prevent neural networks from overfitting, J. Mach. Learn. Res. **15**, 1929 (2014).

[65] G. Cowan, K. Cranmer, E. Gross, and O. Vitells, Asymptotic formulae for likelihood-based tests of new physics, Eur. Phys. J. C **71**, 1554 (2011).

[66] ATLAS Collaboration, Measurement of the inelastic proton–proton cross section at $\sqrt{s} = 13$ TeV with the ATLAS detector at the LHC, Phys. Rev. Lett. **117**, 182002 (2016).

[67] ATLAS Collaboration, Topological cell clustering in the ATLAS calorimeters and its performance in LHC Run 1, Eur. Phys. J. C **77**, 490 (2017).

[68] J. Bellm *et al.*, Herwig 7.0/Herwig++ 3.0 release note, Eur. Phys. J. C **76**, 196 (2016).

[69] A. L. Read, Presentation of search results: The CL_S technique, J. Phys. G **28**, 2693 (2002).

[70] P. Stylianou and G. Weiglein, Constraints on the trilinear and quartic Higgs couplings from triple Higgs production at the LHC and beyond, Eur. Phys. J. C **84**, 366 (2024).

[71] ATLAS Collaboration, ATLAS computing acknowledgements, Report No. ATL-SOFT-PUB-2023-001, 2023, https://cds.cern.ch/record/2869272.

[72] http://hepdata.cedar.ac.uk/

G. Aad[104], E. Aakvaag[17], B. Abbott[123], S. Abdelhameed[119a], K. Abeling[56], N. J. Abicht[50], S. H. Abidi[30], M. Aboelela[46], A. Aboulhorma[36e], H. Abramowicz[155], Y. Abulaiti[120], B. S. Acharya[70a,70b,b], A. Ackermann[64a], C. Adam Bourdarios[4], L. Adamczyk[87a], S. V. Addepalli[147], M. J. Addison[103], J. Adelman[118], A. Adiguzel[22c], T. Adye[137], A. A. Affolder[139], Y. Afik[41], M. N. Agaras[13], A. Aggarwal[102], C. Agheorghiesei[28c], F. Ahmadov[40,c], S. Ahuja[97], X. Ai[63e], G. Aielli[77a,77b], A. Aikot[168], M. Ait Tamlihat[36e], B. Aitbenchikh[36a], M. Akbiyik[102], T. P. A. Åkesson[100], A. V. Akimov[149], D. Akiyama[173], N. N. Akolkar[25], S. Aktas[22a], G. L. Alberghi[24b], J. Albert[170], P. Albicocco[54], G. L. Albouy[61], S. Alderweireldt[53], Z. L. Alegria[124], M. Aleksa[37], I. N. Aleksandrov[40], C. Alexa[28b], T. Alexopoulos[10], F. Alfonsi[24b], M. Algren[57], M. Alhroob[172], B. Ali[135], H. M. J. Ali[93,d], S. Ali[32], S. W. Alibocus[94], M. Aliev[34c], G. Alimonti[72a], W. Alkakhi[56], C. Allaire[67], B. M. M. Allbrooke[150], J. S. Allen[103], J. F. Allen[53], P. P. Allport[21], A. Aloisio[73a,73b], F. Alonso[92], C. Alpigiani[142], Z. M. K. Alsolami[93], A. Alvarez Fernandez[102], M. Alves Cardoso[57], M. G. Alviggi[73a,73b], M. Aly[103], Y. Amaral Coutinho[84b], A. Ambler[106], C. Amelung[37], M. Amerl[103], C. G. Ames[111], D. Amidei[108], B. Amini[55], K. J. Amirie[159], A. Amirkhanov[40], S. P. Amor Dos Santos[133a], K. R. Amos[168], D. Amperiadou[156], S. An[85], V. Ananiev[128], C. Anastopoulos[143], T. Andeen[11], J. K. Anders[94], A. C. Anderson[60], A. Andreazza[72a,72b], S. Angelidakis[9], A. Angerami[43], A. V. Anisenkov[40], A. Annovi[75a], C. Antel[57], E. Antipov[149], M. Antonelli[54]

F. Anulli[76a] M. Aoki[85] T. Aoki[157] M. A. Aparo[150] L. Aperio Bella[49] C. Appelt[155] A. Apyan[27]
S. J. Arbiol Val[88] C. Arcangeletti[54] A. T. H. Arce[52] J-F. Arguin[110] S. Argyropoulos[156] J.-H. Arling[49]
O. Arnaez[4] H. Arnold[149] G. Artoni[76a,76b] H. Asada[113] K. Asai[121] S. Asai[157] N. A. Asbah[37]
R. A. Ashby Pickering[172] A. M. Aslam[97] K. Assamagan[30] R. Astalos[29a] K. S. V. Astrand[100] S. Atashi[163]
R. J. Atkin[34a] H. Atmani,[36f] P. A. Atmasiddha[131] K. Augsten[135] A. D. Auriol[42] V. A. Austrup[103] G. Avolio[37]
K. Axiotis[57] G. Azuelos[110,e] D. Babal[29b] H. Bachacou[138] K. Bachas[156,f] A. Bachiu[35] E. Bachmann[51]
M. J. Backes[64a] A. Badea[41] T. M. Baer[108] P. Bagnaia[76a,76b] M. Bahmani[19] D. Bahner[55] K. Bai[126]
J. T. Baines[137] L. Baines[96] O. K. Baker[177] E. Bakos[16] D. Bakshi Gupta[8] L. E. Balabram Filho[84b]
V. Balakrishnan[123] R. Balasubramanian[4] E. M. Baldin[39] P. Balek[87a] E. Ballabene[24b,24a] F. Balli[138]
L. M. Baltes[64a] W. K. Balunas[33] J. Balz[102] I. Bamwidhi[119b] E. Banas[88] M. Bandieramonte[132]
A. Bandyopadhyay[25] S. Bansal[25] L. Barak[155] M. Barakat[49] E. L. Barberio[107] D. Barberis[58b,58a]
M. Barbero[104] M. Z. Barel[117] T. Barillari[112] M-S. Barisits[37] T. Barklow[147] P. Baron[125]
D. A. Baron Moreno[103] A. Baroncelli[63a] A. J. Barr[129] J. D. Barr[98] F. Barreiro[101]
J. Barreiro Guimarães da Costa[14] M. G. Barros Teixeira[133a] S. Barsov[39] F. Bartels[64a] R. Bartoldus[147]
A. E. Barton[93] P. Bartos[29a] A. Basan[102] M. Baselga[50] S. Bashiri,[88] A. Bassalat[67,g] M. J. Basso[160a]
S. Bataju[46] R. Bate[169] R. L. Bates[60] S. Batlamous,[101] M. Battaglia[139] D. Battulga[19] M. Bauce[76a,76b]
M. Bauer[80] P. Bauer[25] L. T. Bayer[49] L. T. Bazzano Hurrell[31] J. B. Beacham[112] T. Beau[130] J. Y. Beaucamp[92]
P. H. Beauchemin[162] P. Bechtle[25] H. P. Beck[20,h] K. Becker[172] A. J. Beddall[83] V. A. Bednyakov[40]
C. P. Bee[149] L. J. Beemster[16] M. Begalli[84d] M. Begel[30] J. K. Behr[49] J. F. Beirer[37] F. Beisiegel[25]
M. Belfkir[119b] G. Bella[155] L. Bellagamba[24b] A. Bellerive[35] P. Bellos[21] K. Beloborodov[39]
D. Benchekroun[36a] F. Bendebba[36a] Y. Benhammou[155] K. C. Benkendorfer[62] L. Beresford[49] M. Beretta[54]
E. Bergeaas Kuutmann[166] N. Berger[4] B. Bergmann[135] J. Beringer[18a] G. Bernardi[5] C. Bernius[147]
F. U. Bernlochner[25] F. Bernon[37] A. Berrocal Guardia[13] T. Berry[97] P. Berta[136] A. Berthold[51] S. Bethke[112]
A. Betti[76a,76b] A. J. Bevan[96] N. K. Bhalla[55] S. Bharthuar[112] S. Bhatta[149] D. S. Bhattacharya[171]
P. Bhattarai[147] Z. M. Bhatti[120] K. D. Bhide[55] V. S. Bhopatkar[124] R. M. Bianchi[132] G. Bianco[24b,24a]
O. Biebel[111] M. Biglietti[78a] C. S. Billingsley[46] Y. Bimgdi[36f] M. Bindi[56] A. Bingham[176] A. Bingul[22b]
C. Bini[76a,76b] G. A. Bird[33] M. Birman[174] M. Biros[136] S. Biryukov[150] T. Bisanz[50] E. Bisceglie[45b,45a]
J. P. Biswal[137] D. Biswas[145] I. Bloch[49] A. Blue[60] U. Blumenschein[96] J. Blumenthal[102] V. S. Bobrovnikov[40]
M. Boehler[55] B. Boehm[171] D. Bogavac[37] A. G. Bogdanchikov[39] L. S. Boggia[130] V. Boisvert[97] P. Bokan[37]
T. Bold[87a] M. Bomben[5] M. Bona[96] M. Boonekamp[138] A. G. Borbély[60] I. S. Bordulev[39] G. Borissov[93]
D. Bortoletto[129] D. Boscherini[24b] M. Bosman[13] K. Bouaouda[36a] N. Bouchhar[168] L. Boudet[4] J. Boudreau[132]
E. V. Bouhova-Thacker[93] D. Boumediene[42] R. Bouquet[58b,58a] A. Boveia[122] J. Boyd[37] D. Boye[30]
I. R. Boyko[40] L. Bozianu[57] J. Bracinik[21] N. Brahimi[4] G. Brandt[176] O. Brandt[33] B. Brau[105] J. E. Brau[126]
R. Brener[174] L. Brenner[117] R. Brenner[166] S. Bressler[174] G. Brianti[79a,79b] D. Britton[60] D. Britzger[112]
I. Brock[25] R. Brock[109] G. Brooijmans[43] A. J. Brooks,[69] E. M. Brooks[160b] E. Brost[30] L. M. Brown[170]
L. E. Bruce[62] T. L. Bruckler[129] P. A. Bruckman de Renstrom[88] B. Brüers[49] A. Bruni[24b] G. Bruni[24b]
D. Brunner[48a,48b] M. Bruschi[24b] N. Bruscino[76a,76b] T. Buanes[17] Q. Buat[142] D. Buchin[112] A. G. Buckley[60]
O. Bulekov[39] B. A. Bullard[147] S. Burdin[94] C. D. Burgard[50] A. M. Burger[37] B. Burghgrave[8]
O. Burlayenko[55] J. Burleson[167] J. T. P. Burr[33] J. C. Burzynski[146] E. L. Busch[43] V. Büscher[102] P. J. Bussey[60]
J. M. Butler[26] C. M. Buttar[60] J. M. Butterworth[98] W. Buttinger[137] C. J. Buxo Vazquez[109] A. R. Buzykaev[40]
S. Cabrera Urbán[168] L. Cadamuro[67] D. Caforio[59] H. Cai[132] Y. Cai[24b,114c,24a] Y. Cai[114a] V. M. M. Cairo[37]
O. Cakir[3a] N. Calace[37] P. Calafiura[18a] G. Calderini[130] P. Calfayan[35] G. Callea[60] L. P. Caloba[84b] D. Calvet[42]
S. Calvet[42] R. Camacho Toro[130] S. Camarda[37] D. Camarero Munoz[27] P. Camarri[77a,77b] M. T. Camerlingo[73a,73b]
D. Cameron[37] C. Camincher[170] M. Campanelli[98] A. Camplani[44] V. Canale[73a,73b] A. C. Canbay[3a]
E. Canonero[97] J. Cantero[168] Y. Cao[167] F. Capocasa[27] M. Capua[45b,45a] A. Carbone[72a,72b] R. Cardarelli[77a]
J. C. J. Cardenas[8] M. P. Cardiff[27] G. Carducci[45b,45a] T. Carli[37] G. Carlino[73a] J. I. Carlotto[13] B. T. Carlson[132,i]
E. M. Carlson[170] J. Carmignani[94] L. Carminati[72a,72b] A. Carnelli[138] M. Carnesale[37] S. Caron[116]
E. Carquin[140f] I. B. Carr[107] S. Carrá[72a] G. Carratta[24b,24a] A. M. Carroll[126] M. P. Casado[13,j] M. Caspar[49]
F. L. Castillo[4] L. Castillo Garcia[13] V. Castillo Gimenez[168] N. F. Castro[133a,133e] A. Catinaccio[37]

J. R. Catmore[128] T. Cavaliere[4] V. Cavaliere[30] L. J. Caviedes Betancourt[23b] Y. C. Cekmecelioglu[49] E. Celebi[83] S. Cella[37] V. Cepaitis[57] K. Cerny[125] A. S. Cerqueira[84a] A. Cerri[75a,75b] L. Cerrito[77a,77b] F. Cerutti[18a] B. Cervato[145] A. Cervelli[24b] G. Cesarini[54] S. A. Cetin[83] P. M. Chabrillat[130] J. Chan[18a] W. Y. Chan[157] J. D. Chapman[33] E. Chapon[138] B. Chargeishvili[153b] D. G. Charlton[21] C. Chauhan[136] Y. Che[114a] S. Chekanov[6] S. V. Chekulaev[160a] G. A. Chelkov[40,k] B. Chen[155] B. Chen[170] H. Chen[114a] H. Chen[30] J. Chen[63c] J. Chen[146] M. Chen[129] S. Chen[89] S. J. Chen[114a] X. Chen[63c] X. Chen[15,l] C. L. Cheng[175] H. C. Cheng[65a] S. Cheong[147] A. Cheplakov[40] E. Cheremushkina[49] E. Cherepanova[117] R. Cherkaoui El Moursli[36e] E. Cheu[7] K. Cheung[66] L. Chevalier[138] V. Chiarella[54] G. Chiarelli[75a] N. Chiedde[104] G. Chiodini[71a] A. S. Chisholm[21] A. Chitan[28b] M. Chitishvili[168] M. V. Chizhov[40,m] K. Choi[11] Y. Chou[142] E. Y. S. Chow[116] K. L. Chu[174] M. C. Chu[65a] X. Chu[14,114c] Z. Chubinidze[54] J. Chudoba[134] J. J. Chwastowski[88] D. Cieri[112] K. M. Ciesla[87a] V. Cindro[95] A. Ciocio[18a] F. Cirotto[73a,73b] Z. H. Citron[174] M. Citterio[72a] D. A. Ciubotaru[28b] A. Clark[57] P. J. Clark[53] N. Clarke Hall[98] C. Clarry[159] S. E. Clawson[49] C. Clement[48a,48b] Y. Coadou[104] M. Cobal[70a,70c] A. Coccaro[58b] R. F. Coelho Barrue[133a] R. Coelho Lopes De Sa[105] S. Coelli[72a] L. S. Colangeli[159] B. Cole[43] P. Collado Soto[101] J. Collot[61] P. Conde Muiño[133a,133g] M. P. Connell[34c] S. H. Connell[34c] E. I. Conroy[129] F. Conventi[73a,n] H. G. Cooke[21] A. M. Cooper-Sarkar[129] F. A. Corchia[24b,24a] A. Cordeiro Oudot Choi[130] L. D. Corpe[42] M. Corradi[76a,76b] F. Corriveau[106,o] A. Cortes-Gonzalez[19] M. J. Costa[168] F. Costanza[4] D. Costanzo[143] B. M. Cote[122] J. Couthures[4] G. Cowan[97] K. Cranmer[175] L. Cremer[50] D. Cremonini[24b,24a] S. Crépé-Renaudin[61] F. Crescioli[130] M. Cristinziani[145] M. Cristoforetti[79a,79b] V. Croft[117] J. E. Crosby[124] G. Crosetti[45b,45a] A. Cueto[101] H. Cui[98] Z. Cui[7] W. R. Cunningham[60] F. Curcio[168] J. R. Curran[53] P. Czodrowski[37] M. J. Da Cunha Sargedas De Sousa[58b,58a] J. V. Da Fonseca Pinto[84b] C. Da Via[103] W. Dabrowski[87a] T. Dado[37] S. Dahbi[152] T. Dai[108] D. Dal Santo[20] C. Dallapiccola[105] M. Dam[44] G. D'amen[30] V. D'Amico[111] J. Damp[102] J. R. Dandoy[35] D. Dannheim[37] M. Danninger[146] V. Dao[149] G. Darbo[58b] S. J. Das[30] F. Dattola[49] S. D'Auria[72a,72b] A. D'Avanzo[73a,73b] T. Davidek[136] I. Dawson[96] H. A. Day-hall[135] K. De[8] C. De Almeida Rossi[159] R. De Asmundis[73a] N. De Biase[49] S. De Castro[24b,24a] N. De Groot[116] P. de Jong[117] H. De la Torre[118] A. De Maria[114a] A. De Salvo[76a] U. De Sanctis[77a,77b] F. De Santis[71a,71b] A. De Santo[150] J. B. De Vivie De Regie[61] J. Debevc[95] D. V. Dedovich[40] J. Degens[94] A. M. Deiana[46] J. Del Peso[101] L. Delagrange[130] F. Deliot[138] C. M. Delitzsch[50] M. Della Pietra[73a,73b] D. Della Volpe[57] A. Dell'Acqua[37] L. Dell'Asta[72a,72b] M. Delmastro[4] C. C. Delogu[102] P. A. Delsart[61] S. Demers[177] M. Demichev[40] S. P. Denisov[39] H. Denizli[22a,p] L. D'Eramo[42] D. Derendarz[88] F. Derue[130] P. Dervan[94] K. Desch[25] C. Deutsch[25] F. A. Di Bello[58b,58a] A. Di Ciaccio[77a,77b] L. Di Ciaccio[4] A. Di Domenico[76a,76b] C. Di Donato[73a,73b] A. Di Girolamo[37] G. Di Gregorio[37] A. Di Luca[79a,79b] B. Di Micco[78a,78b] R. Di Nardo[78a,78b] K. F. Di Petrillo[41] M. Diamantopoulou[35] F. A. Dias[117] T. Dias Do Vale[146] M. A. Diaz[140a,140b] A. R. Didenko[40] M. Didenko[168] E. B. Diehl[108] S. Díez Cornell[49] C. Diez Pardos[145] C. Dimitriadi[148] A. Dimitrievska[21] A. Dimri[149] J. Dingfelder[25] T. Dingley[129] I-M. Dinu[28b] S. J. Dittmeier[64b] F. Dittus[37] M. Divisek[136] B. Dixit[94] F. Djama[104] T. Djobava[153b] C. Doglioni[103,100] A. Dohnalova[29a] Z. Dolezal[136] K. Domijan[87a] K. M. Dona[41] M. Donadelli[84d] B. Dong[109] J. Donini[42] A. D'Onofrio[73a,73b] M. D'Onofrio[94] J. Dopke[137] A. Doria[73a] N. Dos Santos Fernandes[133a] P. Dougan[103] M. T. Dova[92] A. T. Doyle[60] M. A. Draguet[129] M. P. Drescher[56] E. Dreyer[174] I. Drivas-koulouris[10] M. Drnevich[120] M. Drozdova[57] D. Du[63a] T. A. du Pree[117] F. Dubinin[39] M. Dubovsky[29a] E. Duchovni[174] G. Duckeck[111] O. A. Ducu[28b] D. Duda[53] A. Dudarev[37] E. R. Duden[27] M. D'uffizi[103] L. Duflot[67] M. Dührssen[37] I. Duminica[28g] A. E. Dumitriu[28b] M. Dunford[64a] S. Dungs[50] K. Dunne[48a,48b] A. Duperrin[104] H. Duran Yildiz[3a] M. Düren[59] A. Durglishvili[153b] D. Duvnjak[35] B. L. Dwyer[118] G. I. Dyckes[18a] M. Dyndal[87a] B. S. Dziedzic[37] Z. O. Earnshaw[150] G. H. Eberwein[129] B. Eckerova[29a] S. Eggebrecht[56] E. Egidio Purcino De Souza[84e] G. Eigen[17] K. Einsweiler[18a] T. Ekelof[166] P. A. Ekman[100] S. El Farkh[36b] Y. El Ghazali[63a] H. El Jarrari[37] A. El Moussaouy[36a] V. Ellajosyula[166] M. Ellert[166] F. Ellinghaus[176] N. Ellis[37] J. Elmsheuser[30] M. Elsawy[119a] M. Elsing[37] D. Emeliyanov[137] Y. Enari[85] I. Ene[18a] S. Epari[13] D. Ernani Martins Neto[88] M. Errenst[176] M. Escalier[67] C. Escobar[168] E. Etzion[155] G. Evans[133a,133b] H. Evans[69] L. S. Evans[97] A. Ezhilov[39] S. Ezzarqtouni[36a] F. Fabbri[24b,24a] L. Fabbri[24b,24a] G. Facini[98] V. Fadeyev[139] R. M. Fakhrutdinov[39] D. Fakoudis[102]

S. Falciano[76a] L. F. Falda Ulhoa Coelho[133a] F. Fallavollita[112] G. Falsetti[45b,45a] J. Faltova[136] C. Fan[167] K. Y. Fan[65b] Y. Fan[14] Y. Fang[14,114c] M. Fanti[72a,72b] M. Faraj[70a,70b] Z. Farazpay[99] A. Farbin[8] A. Farilla[78a] T. Farooque[109] J. N. Farr[177] S. M. Farrington[137,53] F. Fassi[36e] D. Fassouliotis[9] L. Fayard[67] P. Federic[136] P. Federicova[134] O. L. Fedin[39,k] M. Feickert[175] L. Feligioni[104] D. E. Fellers[126] C. Feng[63b] Z. Feng[117] M. J. Fenton[163] L. Ferencz[49] P. Fernandez Martinez[68] M. J. V. Fernoux[104] J. Ferrando[93] A. Ferrari[166] P. Ferrari[117,116] R. Ferrari[74a] D. Ferrere[57] C. Ferretti[108] M. P. Fewell[1] D. Fiacco[76a,76b] F. Fiedler[102] P. Fiedler[135] S. Filimonov[39] A. Filipčič[95] E. K. Filmer[160a] F. Filthaut[116] M. C. N. Fiolhais[133a,133c,q] L. Fiorini[168] W. C. Fisher[109] T. Fitschen[103] P. M. Fitzhugh,[138] I. Fleck[145] P. Fleischmann[108] T. Flick,[176] M. Flores[34d,r] L. R. Flores Castillo[65a] L. Flores Sanz De Acedo[37] F. M. Follega[79a,79b] N. Fomin[33] J. H. Foo[159] A. Formica[138] A. C. Forti[103] E. Fortin[37] A. W. Fortman[18a] L. Fountas[9,s] D. Fournier[67] H. Fox[93] P. Francavilla[75a,75b] S. Francescato[62] S. Franchellucci[57] M. Franchini[24b,24a] S. Franchino[64a] D. Francis,[37] L. Franco[116] V. Franco Lima[37] L. Franconi[49] M. Franklin[62] G. Frattari[27] Y. Y. Frid[155] J. Friend[60] N. Fritzsche[37] A. Froch[57] D. Froidevaux[37] J. A. Frost[129] Y. Fu[109] S. Fuenzalida Garrido[140f] M. Fujimoto[104] K. Y. Fung[65a] E. Furtado De Simas Filho[84e] M. Furukawa[157] J. Fuster[168] A. Gaa[56] A. Gabrielli[24b,24a] A. Gabrielli[159] P. Gadow[37] G. Gagliardi[58b,58a] L. G. Gagnon[18a] S. Gaid[165] S. Galantzan[155] J. Gallagher[1] E. J. Gallas[129] A. L. Gallen[166] B. J. Gallop[137] K. K. Gan[122] S. Ganguly[157] Y. Gao[53] A. Garabaglu[142] F. M. Garay Walls[140a,140b] B. Garcia,[30] C. García[168] A. Garcia Alonso[117] A. G. Garcia Caffaro[177] J. E. García Navarro[168] M. Garcia-Sciveres[18a] G. L. Gardner[131] R. W. Gardner[41] N. Garelli[162] R. B. Garg[147] J. M. Gargan[53] C. A. Garner,[159] C. M. Garvey[34a] V. K. Gassmann,[162] G. Gaudio[74a] V. Gautam,[13] P. Gauzzi[76a,76b] J. Gavranovic[95] I. L. Gavrilenko[39] A. Gavrilyuk[39] C. Gay[169] G. Gaycken[126] E. N. Gazis[10] A. Gekow,[122] C. Gemme[58b] M. H. Genest[61] A. D. Gentry[115] S. George[97] W. F. George[21] T. Geralis[47] A. A. Gerwin[123] P. Gessinger-Befurt[37] M. E. Geyik[176] M. Ghani[172] K. Ghorbanian[96] A. Ghosal[145] A. Ghosh[163] A. Ghosh[7] B. Giacobbe[24b] S. Giagu[76a,76b] T. Giani[117] A. Giannini[63a] S. M. Gibson[97] M. Gignac[139] D. T. Gil[87b] A. K. Gilbert[87a] B. J. Gilbert[43] D. Gillberg[35] G. Gilles[117] L. Ginabat[130] D. M. Gingrich[2,e] M. P. Giordani[70a,70c] P. F. Giraud[138] G. Giugliarelli[70a,70c] D. Giugni[72a] F. Giuli[77a,77b] I. Gkialas[9,s] L. K. Gladilin[39] C. Glasman[101] G. Glemža[49] M. Glisic,[126] I. Gnesi[45b] Y. Go[30] M. Goblirsch-Kolb[37] B. Gocke,[50] D. Godin,[110] B. Gokturk[22a] S. Goldfarb[107] T. Golling[57] M. G. D. Gololo[34c] D. Golubkov[39] J. P. Gombas[109] A. Gomes[133a,133b] G. Gomes Da Silva[145] A. J. Gomez Delegido[168] R. Gonçalo[133a] L. Gonella[21] A. Gongadze[153c] F. Gonnella[21] J. L. Gonski[147] R. Y. González Andana[53] S. González de la Hoz[168] R. Gonzalez Lopez[94] C. Gonzalez Renteria[18a] M. V. Gonzalez Rodrigues[49] R. Gonzalez Suarez[166] S. Gonzalez-Sevilla[57] L. Goossens[37] B. Gorini[37] E. Gorini[71a,71b] A. Gorišek[95] T. C. Gosart[131] A. T. Goshaw[52] M. I. Gostkin[40] S. Goswami[124] C. A. Gottardo[37] S. A. Gotz[111] M. Gouighri[36b] A. G. Goussiou[142] N. Govender[34c] R. P. Grabarczyk[129] I. Grabowska-Bold[87a] K. Graham[35] E. Gramstad[128] S. Grancagnolo[71a,71b] C. M. Grant,[1,138] P. M. Gravila[28f] F. G. Gravili[71a,71b] H. M. Gray[18a] M. Greco[112] M. J. Green[1] C. Grefe[25] A. S. Grefsrud[17] I. M. Gregor[49] K. T. Greif[163] P. Grenier[147] S. G. Grewe,[112] A. A. Grillo[139] K. Grimm[32] S. Grinstein[13,t] J.-F. Grivaz[67] E. Gross[174] J. Grosse-Knetter[56] L. Guan[108] G. Guerrieri[37] R. Gugel[102] J. A. M. Guhit[108] A. Guida[19] E. Guilloton[172] S. Guindon[37] F. Guo[14,114c] J. Guo[63c] L. Guo[49] L. Guo[114b,u] Y. Guo[108] A. Gupta[50] R. Gupta[132] S. Gurbuz[25] S. S. Gurdasani[49] G. Gustavino[76a,76b] P. Gutierrez[123] L. F. Gutierrez Zagazeta[131] M. Gutsche[51] C. Gutschow[98] C. Gwenlan[129] C. B. Gwilliam[94] E. S. Haaland[128] A. Haas[120] M. Habedank[60] C. Haber[18a] H. K. Hadavand[8] A. Haddad[42] A. Hadef[51] A. I. Hagan[93] J. J. Hahn[145] E. H. Haines[98] M. Haleem[171] J. Haley[124] G. D. Hallewell[104] L. Halser[20] K. Hamano[170] M. Hamer[25] E. J. Hampshire[97] J. Han[63b] L. Han[114a] L. Han[63a] S. Han[18a] K. Hanagaki[85] M. Hance[139] D. A. Hangal[43] H. Hanif[146] M. D. Hank[131] J. B. Hansen[44] P. H. Hansen[44] D. Harada[57] T. Harenberg[176] S. Harkusha[178] M. L. Harris[105] Y. T. Harris[25] J. Harrison[13] N. M. Harrison[122] P. F. Harrison,[172] N. M. Hartman[112] N. M. Hartmann[111] R. Z. Hasan[97,137] Y. Hasegawa[144] F. Haslbeck[129] S. Hassan[17] R. Hauser[109] C. M. Hawkes[21] R. J. Hawkings[37] Y. Hayashi[157] D. Hayden[109] C. Hayes[108] R. L. Hayes[117] C. P. Hays[129] J. M. Hays[96] H. S. Hayward[94] F. He[63a] M. He[14,114c] Y. He[49] Y. He[98] N. B. Heatley[96] V. Hedberg[100] A. L. Heggelund[128] C. Heidegger[55] K. K. Heidegger[55] J. Heilman[35] S. Heim[49] T. Heim[18a] J. G. Heinlein[131] J. J. Heinrich[126] L. Heinrich[112,v]

J. Hejbal,[134] A. Held,[175] S. Hellesund,[17] C. M. Helling,[169] S. Hellman,[48a,48b] L. Henkelmann,[33]
A. M. Henriques Correia,[37] H. Herde,[100] Y. Hernández Jiménez,[149] L. M. Herrmann,[25] T. Herrmann,[51] G. Herten,[55]
R. Hertenberger,[111] L. Hervas,[37] M. E. Hesping,[102] N. P. Hessey,[160a] J. Hessler,[112] M. Hidaoui,[36b] N. Hidic,[136]
E. Hill,[159] S. J. Hillier,[21] J. R. Hinds,[109] F. Hinterkeuser,[25] M. Hirose,[127] S. Hirose,[161] D. Hirschbuehl,[176]
T. G. Hitchings,[103] B. Hiti,[95] J. Hobbs,[149] R. Hobincu,[28e] N. Hod,[174] M. C. Hodgkinson,[143] B. H. Hodkinson,[129]
A. Hoecker,[37] D. D. Hofer,[108] J. Hofer,[168] M. Holzbock,[37] L. B. A. H. Hommels,[33] B. P. Honan,[103] J. J. Hong,[69]
J. Hong,[63c] T. M. Hong,[132] B. H. Hooberman,[167] W. H. Hopkins,[6] M. C. Hoppesch,[167] Y. Horii,[113]
M. E. Horstmann,[112] S. Hou,[152] M. R. Housenga,[167] A. S. Howard,[95] J. Howarth,[60] J. Hoya,[6] M. Hrabovsky,[125]
T. Hryn'ova,[4] P. J. Hsu,[66] S.-C. Hsu,[142] T. Hsu,[67] M. Hu,[18a] Q. Hu,[63a] S. Huang,[33] X. Huang,[14,114c]
Y. Huang,[136] Y. Huang,[114b] Y. Huang,[102] Y. Huang,[14] Z. Huang,[103] Z. Hubacek,[135] M. Huebner,[25]
F. Huegging,[25] T. B. Huffman,[129] M. Hufnagel Maranha De Faria,[84a] C. A. Hugli,[49] M. Huhtinen,[37]
S. K. Huiberts,[17] R. Hulsken,[106] C. E. Hultquist,[18a] N. Huseynov,[12,w] J. Huston,[109] J. Huth,[62] R. Hyneman,[7]
G. Iacobucci,[57] G. Iakovidis,[30] L. Iconomidou-Fayard,[67] J. P. Iddon,[37] P. Iengo,[73a,73b] R. Iguchi,[157] Y. Iiyama,[157]
T. Iizawa,[129] Y. Ikegami,[85] D. Iliadis,[156] N. Ilic,[159] H. Imam,[84c] G. Inacio Goncalves,[84d]
S. A. Infante Cabanas,[140c] T. Ingebretsen Carlson,[48a,48b] J. M. Inglis,[96] G. Introzzi,[74a,74b] M. Iodice,[78a]
V. Ippolito,[76a,76b] R. K. Irwin,[94] M. Ishino,[157] W. Islam,[175] C. Issever,[19] S. Istin,[22a,x] H. Ito,[173] R. Iuppa,[79a,79b]
A. Ivina,[174] V. Izzo,[73a] P. Jacka,[134] P. Jackson,[1] P. Jain,[49] K. Jakobs,[55] T. Jakoubek,[174] J. Jamieson,[60]
W. Jang,[157] M. Javurkova,[105] P. Jawahar,[103] L. Jeanty,[126] J. Jejelava,[153a] P. Jenni,[55,y] C. E. Jessiman,[35]
C. Jia,[63b] H. Jia,[169] J. Jia,[149] X. Jia,[14,114c] Z. Jia,[114a] C. Jiang,[53] Q. Jiang,[65b] S. Jiggins,[49] J. Jimenez Pena,[13]
S. Jin,[114a] A. Jinaru,[28b] O. Jinnouchi,[141] P. Johansson,[143] K. A. Johns,[7] J. W. Johnson,[139] F. A. Jolly,[49]
D. M. Jones,[150] E. Jones,[49] K. S. Jones,[8] P. Jones,[33] R. W. L. Jones,[93] T. J. Jones,[94] H. L. Joos,[56,37] R. Joshi,[122]
J. Jovicevic,[16] X. Ju,[18a] J. J. Junggeburth,[37] T. Junkermann,[64a] A. Juste Rozas,[13,t] M. K. Juzek,[88] S. Kabana,[140e]
A. Kaczmarska,[88] M. Kado,[112] H. Kagan,[122] M. Kagan,[147] A. Kahn,[131] C. Kahra,[102] T. Kaji,[157]
E. Kajomovitz,[154] N. Kakati,[174] I. Kalaitzidou,[55] N. J. Kang,[139] D. Kar,[34g] K. Karava,[129] E. Karentzos,[25]
O. Karkout,[117] S. N. Karpov,[40] Z. M. Karpova,[40] V. Kartvelishvili,[93] A. N. Karyukhin,[39] E. Kasimi,[156]
J. Katzy,[49] S. Kaur,[35] K. Kawade,[144] M. P. Kawale,[123] C. Kawamoto,[89] T. Kawamoto,[63a] E. F. Kay,[37]
F. I. Kaya,[162] S. Kazakos,[109] V. F. Kazanin,[39] Y. Ke,[149] J. M. Keaveney,[34a] R. Keeler,[170] G. V. Kehris,[62]
J. S. Keller,[35] J. J. Kempster,[150] O. Kepka,[134] J. Kerr,[160b] B. P. Kerridge,[137] B. P. Kerševan,[95] L. Keszeghova,[29a]
R. A. Khan,[132] A. Khanov,[124] A. G. Kharlamov,[39] T. Kharlamova,[39] E. E. Khoda,[142] M. Kholodenko,[133a]
T. J. Khoo,[19] G. Khoriauli,[171] J. Khubua,[153b,a] Y. A. R. Khwaira,[130] B. Kibirige,[34g] D. Kim,[6] D. W. Kim,[48a,48b]
Y. K. Kim,[41] N. Kimura,[98] M. K. Kingston,[56] A. Kirchhoff,[56] C. Kirfel,[25] F. Kirfel,[25] J. Kirk,[137]
A. E. Kiryunin,[112] S. Kita,[161] C. Kitsaki,[10] O. Kivernyk,[25] M. Klassen,[162] C. Klein,[35] L. Klein,[171]
M. H. Klein,[46] S. B. Klein,[57] U. Klein,[94] A. Klimentov,[30] T. Klioutchnikova,[37] P. Kluit,[117] S. Kluth,[112]
E. Kneringer,[80] T. M. Knight,[159] A. Knue,[50] D. Kobylianskii,[174] S. F. Koch,[129] M. Kocian,[147] P. Kodyš,[136]
D. M. Koeck,[126] P. T. Koenig,[25] T. Koffas,[35] O. Kolay,[51] I. Koletsou,[4] T. Komarek,[88] K. Köneke,[56]
A. X. Y. Kong,[1] T. Kono,[121] N. Konstantinidis,[98] P. Kontaxakis,[57] B. Konya,[100] R. Kopeliansky,[43]
S. Koperny,[87a] K. Korcyl,[88] K. Kordas,[156,z] A. Korn,[98] S. Korn,[56] I. Korolkov,[13] N. Korotkova,[39]
B. Kortman,[117] O. Kortner,[112] S. Kortner,[112] W. H. Kostecka,[118] V. V. Kostyukhin,[145] A. Kotsokechagia,[37]
A. Kotwal,[52] A. Koulouris,[37] A. Kourkoumeli-Charalampidi,[74a,74b] C. Kourkoumelis,[9] E. Kourlitis,[112,v]
O. Kovanda,[126] R. Kowalewski,[170] W. Kozanecki,[126] A. S. Kozhin,[39] V. A. Kramarenko,[39] G. Kramberger,[95]
P. Kramer,[25] M. W. Krasny,[130] A. Krasznahorkay,[105] A. C. Kraus,[118] J. W. Kraus,[176] J. A. Kremer,[49] T. Kresse,[51]
L. Kretschmann,[176] J. Kretzschmar,[94] K. Kreul,[19] P. Krieger,[159] K. Krizka,[21] K. Kroeninger,[50] H. Kroha,[112]
J. Kroll,[134] J. Kroll,[131] K. S. Krowpman,[109] U. Kruchonak,[40] H. Krüger,[25] N. Krumnack,[82] M. C. Kruse,[52]
O. Kuchinskaia,[39] S. Kuday,[3a] S. Kuehn,[37] R. Kuesters,[55] T. Kuhl,[49] V. Kukhtin,[40] Y. Kulchitsky,[40]
S. Kuleshov,[140d,140b] M. Kumar,[34g] N. Kumari,[49] P. Kumari,[160b] A. Kupco,[134] T. Kupfer,[50] A. Kupich,[39]
O. Kuprash,[55] H. Kurashige,[86] L. L. Kurchaninov,[160a] O. Kurdysh,[4] Y. A. Kurochkin,[38] A. Kurova,[39]
M. Kuze,[141] A. K. Kvam,[105] J. Kvita,[125] N. G. Kyriacou,[108] L. A. O. Laatu,[104] C. Lacasta,[168] F. Lacava,[76a,76b]
H. Lacker,[19] D. Lacour,[130] N. N. Lad,[98] E. Ladygin,[40] A. Lafarge,[42] B. Laforge,[130] T. Lagouri,[177]
F. Z. Lahbabi,[36a] S. Lai,[56] J. E. Lambert,[170] S. Lammers,[69] W. Lampl,[7] C. Lampoudis,[156,z] G. Lamprinoudis,[102]

A. N. Lancaster[118] E. Lançon[30] U. Landgraf[55] M. P. J. Landon[96] V. S. Lang[55] O. K. B. Langrekken[128] A. J. Lankford[163] F. Lanni[37] K. Lantzsch[25] A. Lanza[74a] M. Lanzac Berrocal[168] J. F. Laporte[138] T. Lari[72a] F. Lasagni Manghi[24b] M. Lassnig[37] V. Latonova[134] S. D. Lawlor[143] Z. Lawrence[103] R. Lazaridou[172] M. Lazzaroni[72a,72b] H. D. M. Le[109] E. M. Le Boulicaut[177] L. T. Le Pottier[18a] B. Leban[24b,24a] M. LeBlanc[103] F. Ledroit-Guillon[61] S. C. Lee[152] T. F. Lee[94] L. L. Leeuw[34c,aa] M. Lefebvre[170] C. Leggett[18a] G. Lehmann Miotto[37] M. Leigh[57] W. A. Leight[105] W. Leinonen[116] A. Leisos[156,bb] M. A. L. Leite[84c] C. E. Leitgeb[19] R. Leitner[136] K. J. C. Leney[46] T. Lenz[25] S. Leone[75a] C. Leonidopoulos[53] A. Leopold[148] J. H. Lepage Bourbonnais[35] R. Les[109] C. G. Lester[33] M. Levchenko[39] J. Levêque[4] L. J. Levinson[174] G. Levrini[24b,24a] M. P. Lewicki[88] C. Lewis[142] D. J. Lewis[4] L. Lewitt[143] A. Li[30] B. Li[63b] C. Li[108] C-Q. Li[112] H. Li[63a] H. Li[63b] H. Li[103] H. Li[15] H. Li[63b] J. Li[63c] K. Li[14] L. Li[63c] R. Li[177] S. Li[14,114c] S. Li[63d,63c,cc] T. Li[5] X. Li[106] Z. Li[157] Z. Li[14,114c] Z. Li[63a] S. Liang[14,114c] Z. Liang[14] M. Liberatore[138] B. Liberti[77a] K. Lie[65c] J. Lieber Marin[84e] H. Lien[69] H. Lin[108] L. Linden[111] R. E. Lindley[7] J. H. Lindon[2] J. Ling[62] E. Lipeles[131] A. Lipniacka[17] A. Lister[169] J. D. Little[69] B. Liu[14] B. X. Liu[114b] D. Liu[63d,63c] E. H. L. Liu[21] J. K. K. Liu[33] K. Liu[63d] K. Liu[63d,63c] M. Liu[63a] M. Y. Liu[63a] P. Liu[14] Q. Liu[63d,142,63c] X. Liu[63a] X. Liu[63b] Y. Liu[114b,114c] Y. L. Liu[63b] Y. W. Liu[63a] S. L. Lloyd[96] E. M. Lobodzinska[49] P. Loch[7] E. Lodhi[159] T. Lohse[19] K. Lohwasser[143] E. Loiacono[49] J. D. Lomas[21] J. D. Long[43] I. Longarini[163] R. Longo[167] A. Lopez Solis[49] N. A. Lopez-canelas[7] N. Lorenzo Martinez[4] A. M. Lory[111] M. Losada[119a] G. Löschcke Centeno[150] O. Loseva[39] X. Lou[48a,48b] X. Lou[14,114c] A. Lounis[67] P. A. Love[93] G. Lu[14,114c] M. Lu[67] S. Lu[131] Y. J. Lu[152] H. J. Lubatti[142] C. Luci[76a,76b] F. L. Lucio Alves[114a] F. Luehring[69] B. S. Lunday[131] O. Lundberg[148] B. Lund-Jensen[148,a] N. A. Luongo[6] M. S. Lutz[37] A. B. Lux[26] D. Lynn[30] R. Lysak[134] E. Lytken[100] V. Lyubushkin[40] T. Lyubushkina[40] M. M. Lyukova[149] M. Firdaus M. Soberi[53] H. Ma[30] K. Ma[63a] L. L. Ma[63b] W. Ma[63a] Y. Ma[124] J. C. MacDonald[102] P. C. Machado De Abreu Farias[84e] R. Madar[42] T. Madula[98] J. Maeda[86] T. Maeno[30] P. T. Mafa[34c,dd] H. Maguire[143] V. Maiboroda[138] A. Maio[133a,133b,133d] K. Maj[87a] O. Majersky[49] S. Majewski[126] R. Makhmanazarov[39] N. Makovec[67] V. Maksimovic[16] B. Malaescu[130] Pa. Malecki[88] V. P. Maleev[39] F. Malek[61,ee] M. Mali[95] D. Malito[97] U. Mallik[81,a] S. Maltezos[10] S. Malyukov[40] J. Mamuzic[13] G. Mancini[54] M. N. Mancini[27] G. Manco[74a,74b] J. P. Mandalia[96] S. S. Mandarry[150] I. Mandić[95] L. Manhaes de Andrade Filho[84a] I. M. Maniatis[174] J. Manjarres Ramos[91] D. C. Mankad[174] A. Mann[111] S. Manzoni[37] L. Mao[63c] X. Mapekula[34c] A. Marantis[156,bb] G. Marchiori[5] M. Marcisovsky[134] C. Marcon[72a] M. Marinescu[21] S. Marium[49] M. Marjanovic[123] A. Markhoos[55] M. Markovitch[67] M. K. Maroun[105] E. J. Marshall[93] Z. Marshall[18a] S. Marti-Garcia[168] J. Martin[98] T. A. Martin[137] V. J. Martin[53] B. Martin dit Latour[17] L. Martinelli[76a,76b] M. Martinez[13,t] P. Martinez Agullo[168] V. I. Martinez Outschoorn[105] P. Martinez Suarez[13] S. Martin-Haugh[137] G. Martinovicova[136] V. S. Martoiu[28b] A. C. Martyniuk[98] A. Marzin[37] D. Mascione[79a,79b] L. Masetti[102] J. Masik[103] A. L. Maslennikov[40] S. L. Mason[43] P. Massarotti[73a,73b] P. Mastrandrea[75a,75b] A. Mastroberardino[45b,45a] T. Masubuchi[127] T. T. Mathew[126] J. Matousek[136] D. M. Mattern[50] J. Maurer[28b] T. Maurin[60] A. J. Maury[67] B. Maček[95] D. A. Maximov[39] A. E. May[103] E. Mayer[42] R. Mazini[34g] I. Maznas[118] M. Mazza[109] S. M. Mazza[139] E. Mazzeo[72a,72b] J. P. Mc Gowan[170] S. P. Mc Kee[108] C. A. Mc Lean[6] C. C. McCracken[169] E. F. McDonald[107] A. E. McDougall[117] L. F. Mcelhinney[93] J. A. Mcfayden[150] R. P. McGovern[131] R. P. Mckenzie[34g] T. C. Mclachlan[49] D. J. Mclaughlin[98] S. J. McMahon[137] C. M. Mcpartland[94] R. A. McPherson[170,o] S. Mehlhase[111] A. Mehta[94] D. Melini[168] B. R. Mellado Garcia[34g] A. H. Melo[56] F. Meloni[49] A. M. Mendes Jacques Da Costa[103] H. Y. Meng[159] L. Meng[93] S. Menke[112] M. Mentink[37] E. Meoni[45b,45a] G. Mercado[118] S. Merianos[156] C. Merlassino[70a,70c] C. Meroni[72a,72b] J. Metcalfe[6] A. S. Mete[6] E. Meuser[102] C. Meyer[69] J-P. Meyer[138] R. P. Middleton[137] L. Mijović[53] G. Mikenberg[174] M. Mikestikova[134] M. Mikuž[95] H. Mildner[102] A. Milic[37] D. W. Miller[41] E. H. Miller[147] L. S. Miller[35] A. Milov[174] D. A. Milstead[48a,48b] T. Min[114a] A. A. Minaenko[39] I. A. Minashvili[153b] A. I. Mincer[120] B. Mindur[87a] M. Mineev[40] Y. Mino[89] L. M. Mir[13] M. Miralles Lopez[60] M. Mironova[18a] M. C. Missio[116] A. Mitra[172] V. A. Mitsou[168] Y. Mitsumori[113] O. Miu[159] P. S. Miyagawa[96] T. Mkrtchyan[64a] M. Mlinarevic[98] T. Mlinarevic[98] M. Mlynarikova[37] S. Mobius[20] P. Mogg[111] M. H. Mohamed Farook[115] A. F. Mohammed[14,114c] S. Mohapatra[43] S. Mohiuddin[124] G. Mokgatitswane[34g]

L. Moleri[174] B. Mondal[145] S. Mondal[135] K. Mönig[49] E. Monnier[104] L. Monsonis Romero,[168]
J. Montejo Berlingen[13] A. Montella,[48a,48b] M. Montella[122] F. Montereali[78a,78b] F. Monticelli[92] S. Monzani,[70a,70c]
A. Morancho Tarda[44] N. Morange[67] A. L. Moreira De Carvalho[49] M. Moreno Llácer[168] C. Moreno Martinez,[57]
J. M. Moreno Perez,[23b] P. Morettini[58b] S. Morgenstern[37] M. Morii[62] M. Morinaga[157] M. Moritsu,[90]
F. Morodei[76a,76b] P. Moschovakos[37] B. Moser[129] M. Mosidze[153b] T. Moskalets[46] P. Moskvitina,[116]
J. Moss,[32,ff] P. Moszkowicz[87a] A. Moussa[36d] Y. Moyal[174] E. J. W. Moyse[105] O. Mtintsilana[34g] S. Muanza,[104]
J. Mueller[132] R. Müller[37] G. A. Mullier[166] A. J. Mullin[33] J. J. Mullin[52] A. E. Mulski[62] D. P. Mungo,[159]
D. Munoz Perez,[168] F. J. Munoz Sanchez[103] M. Murin[103] W. J. Murray[172,137] M. Muškinja[95] C. Mwewa,[30]
A. G. Myagkov,[39,k] A. J. Myers[8] G. Myers[108] M. Myska[135] B. P. Nachman[18a] K. Nagai[129] K. Nagano,[85]
R. Nagasaka,[157] J. L. Nagle,[30,gg] E. Nagy[104] A. M. Nairz[37] Y. Nakahama[85] K. Nakamura[85] K. Nakkalil,[5]
H. Nanjo[127] E. A. Narayanan[46] Y. Narukawa[157] I. Naryshkin[39] L. Nasella,[72a,72b] S. Nasri[119b] C. Nass,[25]
G. Navarro[23a] J. Navarro-Gonzalez[168] A. Nayaz[19] P. Y. Nechaeva[39] S. Nechaeva,[24b,24a] F. Nechansky,[134]
L. Nedic[129] T. J. Neep[21] A. Negri,[74a,74b] M. Negrini[24b] C. Nellist[117] C. Nelson[106] K. Nelson,[108]
S. Nemecek,[134] M. Nessi,[37,hh] M. S. Neubauer[167] F. Neuhaus[102] J. Newell[94] P. R. Newman[21] Y. W. Y. Ng,[167]
B. Ngair[119a] H. D. N. Nguyen[110] R. B. Nickerson[129] R. Nicolaidou[138] J. Nielsen[139] M. Niemeyer,[56]
J. Niermann,[37] N. Nikiforou[37] V. Nikolaenko,[39,k] I. Nikolic-Audit[130] P. Nilsson[30] I. Ninca,[49] G. Ninio,[155]
A. Nisati,[76a] N. Nishu[2] R. Nisius[112] N. Nitika,[70a,70c] J-E. Nitschke[51] E. K. Nkadimeng[34g] T. Nobe,[157]
T. Nommensen[151] M. B. Norfolk[143] B. J. Norman[35] M. Noury[36a] J. Novak[95] T. Novak[95] R. Novotny,[115]
L. Nozka,[125] K. Ntekas[163] N. M. J. Nunes De Moura Junior[84b] J. Ocariz[130] A. Ochi[86] I. Ochoa,[133a]
S. Oerdek,[49,ii] J. T. Offermann[41] A. Ogrodnik[136] A. Oh[103] C. C. Ohm[148] H. Oide[85] R. Oishi,[157]
M. L. Ojeda[37] Y. Okumura[157] L. F. Oleiro Seabra[133a] I. Oleksiyuk[57] S. A. Olivares Pino,[140d]
G. Oliveira Correa[13] D. Oliveira Damazio[30] J. L. Oliver[163] Ö. O. Öncel[55] A. P. O'Neill[20] A. Onofre,[133a,133e]
P. U. E. Onyisi[11] M. J. Oreglia[41] D. Orestano,[78a,78b] R. S. Orr[159] L. M. Osojnak[131] Y. Osumi,[113]
G. Otero y Garzon[31] H. Otono[90] G. J. Ottino[18a] M. Ouchrif[36d] F. Ould-Saada[128] T. Ovsiannikova,[142]
M. Owen[60] R. E. Owen[137] V. E. Ozcan[22a] F. Ozturk[88] N. Ozturk[8] S. Ozturk[83] H. A. Pacey,[129]
K. Pachal[160a] A. Pacheco Pages[13] C. Padilla Aranda[13] G. Padovano[76a,76b] S. Pagan Griso[18a] G. Palacino,[69]
A. Palazzo,[71a,71b] J. Pampel[25] J. Pan[177] T. Pan[65a] D. K. Panchal[11] C. E. Pandini[117] J. G. Panduro Vazquez,[137]
H. D. Pandya[1] H. Pang[138] P. Pani[49] G. Panizzo,[70a,70c] L. Panwar[130] L. Paolozzi[57] S. Parajuli,[167]
A. Paramonov[6] C. Paraskevopoulos[54] D. Paredes Hernandez[65b] A. Pareti,[74a,74b] K. R. Park[43] T. H. Park,[112]
F. Parodi,[58b,58a] J. A. Parsons[43] U. Parzefall[55] B. Pascual Dias[42] L. Pascual Dominguez[101] E. Pasqualucci,[76a]
S. Passaggio,[58b] F. Pastore[97] P. Patel[88] U. M. Patel[52] J. R. Pater[103] T. Pauly[37] F. Pauwels[136] C. I. Pazos,[162]
M. Pedersen[128] R. Pedro[133a] S. V. Peleganchuk[39] O. Penc[37] E. A. Pender[53] S. Peng[15] G. D. Penn,[177]
K. E. Penski[111] M. Penzin[39] B. S. Peralva[84d] A. P. Pereira Peixoto[142] L. Pereira Sanchez,[147]
D. V. Perepelitsa,[30,gg] G. Perera[105] E. Perez Codina[160a] M. Perganti[10] H. Pernegger[37] S. Perrella,[76a,76b]
O. Perrin[42] K. Peters[49] R. F. Y. Peters[103] B. A. Petersen[37] T. C. Petersen[44] E. Petit[104] V. Petousis,[135]
C. Petridou,[156,z] T. Petru[136] A. Petrukhin[145] M. Pettee[18a] A. Petukhov[83] K. Petukhova[37] R. Pezoa,[140f]
L. Pezzotti,[24b,24a] G. Pezzullo[177] L. Pfaffenbichler[37] A. J. Pfleger[37] T. M. Pham[175] T. Pham,[107]
P. W. Phillips[137] G. Piacquadio[149] E. Pianori[18a] F. Piazza[126] R. Piegaia[31] D. Pietreanu[28b] A. D. Pilkington,[103]
M. Pinamonti,[70a,70c] J. L. Pinfold[2] B. C. Pinheiro Pereira[133a] J. Pinol Bel[13] A. E. Pinto Pinoargote,[138]
L. Pintucci,[70a,70c] K. M. Piper[150] A. Pirttikoski[57] D. A. Pizzi[35] L. Pizzimento[65b] M.-A. Pleier[30] V. Pleskot,[136]
E. Plotnikova,[40] G. Poddar[96] R. Poettgen[100] L. Poggioli[130] S. Polacek[136] G. Polesello[74a] A. Poley,[146,160a]
A. Polini,[24b] C. S. Pollard[172] Z. B. Pollock[122] E. Pompa Pacchi[123] N. I. Pond[98] D. Ponomarenko,[69]
L. Pontecorvo,[37] S. Popa[28a] G. A. Popeneciu[28d] A. Poreba[37] D. M. Portillo Quintero[160a] S. Pospisil,[135]
M. A. Postill,[143] P. Postolache[28c] K. Potamianos[172] P. A. Potepa[87a] I. N. Potrap[40] C. J. Potter[33] H. Potti,[151]
J. Poveda[168] M. E. Pozo Astigarraga[37] A. Prades Ibanez,[77a,77b] J. Pretel[170] D. Price[103] M. Primavera,[71a]
L. Primomo,[70a,70c] M. A. Principe Martin[101] R. Privara[125] T. Procter[60] M. L. Proffitt[142] N. Proklova,[131]
K. Prokofiev,[65c] G. Proto[112] J. Proudfoot[6] M. Przybycien[87a] W. W. Przygoda[87b] A. Psallidas,[47]
J. E. Puddefoot[143] D. Pudzha[55] D. Pyatiizbyantseva[116] J. Qian[108] R. Qian[109] D. Qichen[103] Y. Qin,[13]
T. Qiu[53] A. Quadt[56] M. Queitsch-Maitland[103] G. Quetant[57] R. P. Quinn[169] G. Rabanal Bolanos,[62]

D. Rafanoharana[55] F. Raffaeli[77a,77b] F. Ragusa[72a,72b] J. L. Rainbolt[41] J. A. Raine[57] S. Rajagopalan[30] E. Ramakoti[39] L. Rambelli[58b,58a] I. A. Ramirez-Berend[35] K. Ran[49,114c] D. S. Rankin[131] N. P. Rapheeha[34g] H. Rasheed[28b] V. Raskina[130] D. F. Rassloff[64a] A. Rastogi[18a] S. Rave[102] S. Ravera[58b,58a] B. Ravina[37] I. Ravinovich[174] M. Raymond[37] A. L. Read[128] N. P. Readioff[143] D. M. Rebuzzi[74a,74b] A. S. Reed[112] K. Reeves[27] J. A. Reidelsturz[176] D. Reikher[126] A. Rej[50] C. Rembser[37] H. Ren[63a] M. Renda[28b] F. Renner[49] A. G. Rennie[163] A. L. Rescia[49] S. Resconi[72a] M. Ressegotti[58b,58a] S. Rettie[37] W. F. Rettie[35] J. G. Reyes Rivera[109] E. Reynolds[18a] O. L. Rezanova[40] P. Reznicek[136] H. Riani[36d] N. Ribaric[52] E. Ricci[79a,79b] R. Richter[112] S. Richter[48a,48b] E. Richter-Was[87b] M. Ridel[130] S. Ridouani[36d] P. Rieck[120] P. Riedler[37] E. M. Riefel[48a,48b] J. O. Rieger[117] M. Rijssenbeek[149] M. Rimoldi[37] L. Rinaldi[24b,24a] P. Rincke[56,166] G. Ripellino[166] I. Riu[13] J. C. Rivera Vergara[170] F. Rizatdinova[124] E. Rizvi[96] B. R. Roberts[18a] S. S. Roberts[139] D. Robinson[33] M. Robles Manzano[102] A. Robson[60] A. Rocchi[77a,77b] C. Roda[75a,75b] S. Rodriguez Bosca[37] Y. Rodriguez Garcia[23a] A. M. Rodríguez Vera[118] S. Roe[37] J. T. Roemer[37] O. Røhne[128] C. P. A. Roland[130] J. Roloff[30] A. Romaniouk[80] E. Romano[74a,74b] M. Romano[24b] A. C. Romero Hernandez[167] N. Rompotis[94] L. Roos[130] S. Rosati[76a] B. J. Rosser[41] E. Rossi[129] E. Rossi[73a,73b] L. P. Rossi[62] L. Rossini[55] R. Rosten[122] M. Rotaru[28b] B. Rottler[55] D. Rousseau[67] D. Rousso[49] S. Roy-Garand[159] A. Rozanov[104] Z. M. A. Rozario[60] Y. Rozen[154] A. Rubio Jimenez[168] V. H. Ruelas Rivera[19] T. A. Ruggeri[1] A. Ruggiero[129] A. Ruiz-Martinez[168] A. Rummler[37] Z. Rurikova[55] N. A. Rusakovich[40] H. L. Russell[170] G. Russo[76a,76b] J. P. Rutherfoord[7] S. Rutherford Colmenares[33] M. Rybar[136] E. B. Rye[128] A. Ryzhov[46] J. A. Sabater Iglesias[57] H. F-W. Sadrozinski[139] F. Safai Tehrani[76a] S. Saha[1] M. Sahinsoy[83] A. Saibel[168] B. T. Saifuddin[123] M. Saimpert[138] M. Saito[157] T. Saito[157] A. Sala[72a,72b] D. Salamani[37] A. Salnikov[147] J. Salt[168] A. Salvador Salas[155] D. Salvatore[45b,45a] F. Salvatore[150] A. Salzburger[37] D. Sammel[55] E. Sampson[93] D. Sampsonidis[156,z] D. Sampsonidou[126] J. Sánchez[168] V. Sanchez Sebastian[168] H. Sandaker[128] C. O. Sander[49] J. A. Sandesara[105] M. Sandhoff[176] C. Sandoval[23b] L. Sanfilippo[64a] D. P. C. Sankey[137] T. Sano[89] A. Sansoni[54] L. Santi[37] C. Santoni[42] H. Santos[133a,133b] A. Santra[174] E. Sanzani[24b,24a] K. A. Saoucha[165] J. G. Saraiva[133a,133d] J. Sardain[7] O. Sasaki[85] K. Sato[161] C. Sauer[37] E. Sauvan[4] P. Savard[159,e] R. Sawada[157] C. Sawyer[137] L. Sawyer[99] C. Sbarra[24b] A. Sbrizzi[24b,24a] T. Scanlon[98] J. Schaarschmidt[142] U. Schäfer[102] A. C. Schaffer[67,46] D. Schaile[111] R. D. Schamberger[149] C. Scharf[19] M. M. Schefer[20] V. A. Schegelsky[39] D. Scheirich[136] M. Schernau[140e] C. Scheulen[57] C. Schiavi[58b,58a] M. Schioppa[45b,45a] B. Schlag[147] S. Schlenker[37] J. Schmeing[176] M. A. Schmidt[176] K. Schmieden[102] C. Schmitt[102] N. Schmitt[102] S. Schmitt[49] L. Schoeffel[138] A. Schoening[64b] P. G. Scholer[35] E. Schopf[145] M. Schott[25] S. Schramm[57] T. Schroer[57] H-C. Schultz-Coulon[64a] M. Schumacher[55] B. A. Schumm[139] Ph. Schune[138] H. R. Schwartz[139] A. Schwartzman[147] T. A. Schwarz[108] Ph. Schwemling[138] R. Schwienhorst[109] F. G. Sciacca[20] A. Sciandra[30] G. Sciolla[27] F. Scuri[75a] C. D. Sebastiani[37] K. Sedlaczek[118] S. C. Seidel[115] A. Seiden[139] B. D. Seidlitz[43] C. Seitz[49] J. M. Seixas[84b] G. Sekhniaidze[73a] L. Selem[61] N. Semprini-Cesari[24b,24a] A. Semushin[178,39] D. Sengupta[57] V. Senthilkumar[168] L. Serin[67] M. Sessa[77a,77b] H. Severini[123] F. Sforza[58b,58a] A. Sfyrla[57] Q. Sha[14] E. Shabalina[56] H. Shaddix[118] A. H. Shah[33] R. Shaheen[148] J. D. Shahinian[131] D. Shaked Renous[174] M. Shamim[37] L. Y. Shan[14] M. Shapiro[18a] A. Sharma[37] A. S. Sharma[169] P. Sharma[30] P. B. Shatalov[39] K. Shaw[150] S. M. Shaw[103] Q. Shen[63c] D. J. Sheppard[146] P. Sherwood[98] L. Shi[98] X. Shi[14] S. Shimizu[85] C. O. Shimmin[177] I. P. J. Shipsey[129,a] S. Shirabe[90] M. Shiyakova[40,jj] M. J. Shochet[41] D. R. Shope[128] B. Shrestha[123] S. Shrestha[122,kk] I. Shreyber[39] M. J. Shroff[170] P. Sicho[134] A. M. Sickles[167] E. Sideras Haddad[34g,164] A. C. Sidley[117] A. Sidoti[24b] F. Siegert[51] Dj. Sijacki[16] F. Sili[92] J. M. Silva[53] I. Silva Ferreira[84b] M. V. Silva Oliveira[30] S. B. Silverstein[48a] S. Simion[67] R. Simoniello[37] E. L. Simpson[103] H. Simpson[150] L. R. Simpson[108] S. Simsek[83] S. Sindhu[56] P. Sinervo[159] S. N. Singh[27] S. Singh[30] S. Sinha[49] S. Sinha[103] M. Sioli[24b,24a] K. Sioulas[9] I. Siral[37] E. Sitnikova[49] J. Sjölin[48a,48b] A. Skaf[56] E. Skorda[21] P. Skubic[123] M. Slawinska[88] I. Slazyk[17] V. Smakhtin[174] B. H. Smart[137] S. Yu. Smirnov[140b] Y. Smirnov[39] L. N. Smirnova[39,k] O. Smirnova[100] A. C. Smith[43] D. R. Smith[163] E. A. Smith[41] J. L. Smith[103] M. B. Smith[35] R. Smith[147] H. Smitmanns[102] M. Smizanska[93] K. Smolek[135] A. A. Snesarev[40] H. L. Snoek[117] S. Snyder[30] R. Sobie[170,o] A. Soffer[155] C. A. Solans Sanchez[37] E. Yu. Soldatov[39] U. Soldevila[168] A. A. Solodkov[34g] S. Solomon[27] A. Soloshenko[40] K. Solovieva[55] O. V. Solovyanov[42] P. Sommer[51]

A. Sonay[13] W. Y. Song[160b] A. Sopczak[135] A. L. Sopio[53] F. Sopkova[29b] J. D. Sorenson[115]
I. R. Sotarriva Alvarez[141] V. Sothilingam[64a] O. J. Soto Sandoval[140c,140b] S. Sottocornola[69] R. Soualah[165]
Z. Soumaimi[36e] D. South[49] N. Soybelman[174] S. Spagnolo[71a,71b] M. Spalla[112] D. Sperlich[55] B. Spisso[73a,73b]
D. P. Spiteri[60] M. Spousta[136] E. J. Staats[35] R. Stamen[64a] E. Stanecka[88] W. Stanek-Maslouska[49]
M. V. Stange[51] B. Stanislaus[18a] M. M. Stanitzki[49] B. Stapf[49] E. A. Starchenko[39] G. H. Stark[139] J. Stark[91]
P. Staroba[134] P. Starovoitov[165] R. Staszewski[88] G. Stavropoulos[47] A. Stefl[37] P. Steinberg[30] B. Stelzer[146,160a]
H. J. Stelzer[132] O. Stelzer-Chilton[160a] H. Stenzel[59] T. J. Stevenson[150] G. A. Stewart[37] J. R. Stewart[124]
M. C. Stockton[37] G. Stoicea[28b] M. Stolarski[133a] S. Stonjek[112] A. Straessner[51] J. Strandberg[148]
S. Strandberg[48a,48b] M. Stratmann[176] M. Strauss[123] T. Strebler[104] P. Strizenec[29b] R. Ströhmer[171]
D. M. Strom[126] R. Stroynowski[46] A. Strubig[48a,48b] S. A. Stucci[30] B. Stugu[17] J. Stupak[123] N. A. Styles[49]
D. Su[147] S. Su[63a] W. Su[63d] X. Su[63a] D. Suchy[29a] K. Sugizaki[131] V. V. Sulin[39] M. J. Sullivan[94]
D. M. S. Sultan[129] L. Sultanaliyeva[39] S. Sultansoy[3b] S. Sun[175] W. Sun[14] O. Sunneborn Gudnadottir[166]
N. Sur[104] M. R. Sutton[150] H. Suzuki[161] M. Svatos[134] M. Swiatlowski[160a] T. Swirski[171] I. Sykora[29a]
M. Sykora[136] T. Sykora[136] D. Ta[102] K. Tackmann[49,ii] A. Taffard[163] R. Tafirout[160a] J. S. Tafoya Vargas[67]
Y. Takubo[85] M. Talby[104] A. A. Talyshev[39] K. C. Tam[65b] N. M. Tamir[155] A. Tanaka[157] J. Tanaka[157]
R. Tanaka[67] M. Tanasini[149] Z. Tao[169] S. Tapia Araya[140f] S. Tapprogge[102] A. Tarek Abouelfadl Mohamed[109]
S. Tarem[154] K. Tariq[14] G. Tarna[28b] G. F. Tartarelli[72a] M. J. Tartarin[91] P. Tas[136] M. Tasevsky[134]
E. Tassi[45b,45a] A. C. Tate[167] G. Tateno[157] Y. Tayalati[36e,ll] G. N. Taylor[107] W. Taylor[160b] A. S. Tegetmeier[91]
P. Teixeira-Dias[97] J. J. Teoh[159] K. Terashi[157] J. Terron[101] S. Terzo[13] M. Testa[54] R. J. Teuscher[159,o]
A. Thaler[80] O. Theiner[57] T. Theveneaux-Pelzer[104] O. Thielmann[176] D. W. Thomas[97] J. P. Thomas[21]
E. A. Thompson[18a] P. D. Thompson[21] E. Thomson[131] R. E. Thornberry[46] C. Tian[63a] Y. Tian[57]
V. Tikhomirov[39,k] Yu. A. Tikhonov[39] S. Timoshenko[39] D. Timoshyn[136] E. X. L. Ting[1] P. Tipton[177]
A. Tishelman-Charny[30] S. H. Tlou[34g] K. Todome[141] S. Todorova-Nova[136] S. Todt[51] L. Toffolin[70a,70c]
M. Togawa[85] J. Tojo[90] S. Tokár[29a] O. Toldaiev[69] G. Tolkachev[104] M. Tomoto[85,113] L. Tompkins[147,mm]
E. Torrence[126] H. Torres[91] E. Torró Pastor[168] M. Toscani[31] C. Tosciri[41] M. Tost[11] D. R. Tovey[143]
T. Trefzger[171] A. Tricoli[30] I. M. Trigger[160a] S. Trincaz-Duvoid[130] D. A. Trischuk[27] A. Tropina[40] L. Truong[34c]
M. Trzebinski[88] A. Trzupek[88] F. Tsai[149] M. Tsai[108] A. Tsiamis[156] P. V. Tsiareshka[40] S. Tsigaridas[160a]
A. Tsirigotis[156,bb] V. Tsiskaridze[159] E. G. Tskhadadze[153a] M. Tsopoulou[156] Y. Tsujikawa[89] I. I. Tsukerman[39]
V. Tsulaia[18a] S. Tsuno[85] K. Tsuri[121] D. Tsybychev[149] Y. Tu[65b] A. Tudorache[28b] V. Tudorache[28b]
S. Turchikhin[58b,58a] I. Turk Cakir[3a] R. Turra[72a] T. Turtuvshin[40] P. M. Tuts[43] S. Tzamarias[156,z] E. Tzovara[102]
F. Ukegawa[161] P. A. Ulloa Poblete[140c,140b] E. N. Umaka[30] G. Unal[37] A. Undrus[30] G. Unel[163] J. Urban[29b]
P. Urrejola[140a] G. Usai[8] R. Ushioda[158] M. Usman[110] F. Ustuner[53] Z. Uysal[83] V. Vacek[135] B. Vachon[106]
T. Vafeiadis[37] A. Vaitkus[98] C. Valderanis[111] E. Valdes Santurio[48a,48b] M. Valente[160a] S. Valentinetti[24b,24a]
A. Valero[168] E. Valiente Moreno[168] A. Vallier[91] J. A. Valls Ferrer[168] D. R. Van Arneman[117]
T. R. Van Daalen[142] A. Van Der Graaf[50] H. Z. Van Der Schyf[34g] P. Van Gemmeren[6] M. Van Rijnbach[37]
S. Van Stroud[98] I. Van Vulpen[117] P. Vana[136] M. Vanadia[77a,77b] U. M. Vande Voorde[148] W. Vandelli[37]
E. R. Vandewall[124] D. Vannicola[155] L. Vannoli[54] R. Vari[76a] E. W. Varnes[7] C. Varni[18b] D. Varouchas[67]
L. Varriale[168] K. E. Varvell[151] M. E. Vasile[28b] L. Vaslin[85] A. Vasyukov[40] L. M. Vaughan[124] R. Vavricka[136]
T. Vazquez Schroeder[13] J. Veatch[32] V. Vecchio[103] M. J. Veen[105] I. Veliscek[30] L. M. Veloce[159]
F. Veloso[133a,133c] S. Veneziano[76a] A. Ventura[71a,71b] S. Ventura Gonzalez[138] A. Verbytskyi[112] M. Verducci[75a,75b]
C. Vergis[96] M. Verissimo De Araujo[84b] W. Verkerke[117] J. C. Vermeulen[117] C. Vernieri[147] M. Vessella[163]
M. C. Vetterli[146,e] A. Vgenopoulos[102] N. Viaux Maira[140f] T. Vickey[143] O. E. Vickey Boeriu[143]
G. H. A. Viehhauser[129] L. Vigani[64b] M. Vigl[112] M. Villa[24b,24a] M. Villaplana Perez[168] E. M. Villhauer[53]
E. Vilucchi[54] M. G. Vincter[35] A. Visibile[117] C. Vittori[37] I. Vivarelli[24b,24a] E. Voevodina[112] F. Vogel[111]
J. C. Voigt[51] P. Vokac[135] Yu. Volkotrub[87b] E. Von Toerne[25] B. Vormwald[37] K. Vorobev[39] M. Vos[168]
K. Voss[145] M. Vozak[37] L. Vozdecky[123] N. Vranjes[16] M. Vranjes Milosavljevic[16] M. Vreeswijk[117]
N. K. Vu[63d,63c] R. Vuillermet[37] O. Vujinovic[102] I. Vukotic[41] I. K. Vyas[35] S. Wada[161] C. Wagner[147]
J. M. Wagner[18a] W. Wagner[176] S. Wahdan[176] H. Wahlberg[92] C. H. Waits[123] J. Walder[137] R. Walker[111]
W. Walkowiak[145] A. Wall[131] E. J. Wallin[100] T. Wamorkar[18a] A. Z. Wang[139] C. Wang[102] C. Wang[11]

H. Wang[18a] J. Wang,[65c] P. Wang[103] P. Wang,[98] R. Wang,[62] R. Wang,[6] S. M. Wang,[152] S. Wang,[14] T. Wang,[63a] W. T. Wang,[81] W. Wang,[14] X. Wang,[167] X. Wang,[63c] Y. Wang,[114a] Y. Wang,[63a] Z. Wang,[108] Z. Wang,[63d,52,63c] Z. Wang,[108] C. Wanotayaroj,[85] A. Warburton,[106] R. J. Ward,[21] A. L. Warnerbring,[145] N. Warrack,[60] S. Waterhouse,[97] A. T. Watson,[21] H. Watson,[53] M. F. Watson,[21] E. Watton,[60] G. Watts,[142] B. M. Waugh,[98] J. M. Webb,[55] C. Weber,[30] H. A. Weber,[19] M. S. Weber,[20] S. M. Weber,[64a] C. Wei,[63a] Y. Wei,[55] A. R. Weidberg,[129] E. J. Weik,[120] J. Weingarten,[50] C. Weiser,[55] C. J. Wells,[49] T. Wenaus,[30] B. Wendland,[50] T. Wengler,[37] N. S. Wenke,[112] N. Wermes,[25] M. Wessels,[64a] A. M. Wharton,[93] A. S. White,[62] A. White,[8] M. J. White,[1] D. Whiteson,[163] L. Wickremasinghe,[127] W. Wiedenmann,[175] M. Wielers,[137] C. Wiglesworth,[44] D. J. Wilbern,[123] H. G. Wilkens,[37] J. J. H. Wilkinson,[33] D. M. Williams,[43] H. H. Williams,[131] S. Williams,[33] S. Willocq,[105] B. J. Wilson,[103] D. J. Wilson,[103] P. J. Windischhofer,[41] F. I. Winkel,[31] F. Winklmeier,[126] B. T. Winter,[55] M. Wittgen,[147] M. Wobisch,[99] T. Wojtkowski,[61] Z. Wolffs,[117] J. Wollrath,[37] M. W. Wolter,[88] H. Wolters,[133a,133c] M. C. Wong,[139] E. L. Woodward,[43] S. D. Worm,[49] B. K. Wosiek,[88] K. W. Woźniak,[88] S. Wozniewski,[56] K. Wraight,[60] C. Wu,[21] M. Wu,[114b] M. Wu,[116] S. L. Wu,[175] X. Wu,[57] X. Wu,[63a] Y. Wu,[63a] Z. Wu,[4] J. Wuerzinger,[112,v] T. R. Wyatt,[103] B. M. Wynne,[53] S. Xella,[44] L. Xia,[114a] M. Xia,[15] M. Xie,[63a] A. Xiong,[126] J. Xiong,[18a] D. Xu,[14] H. Xu,[63a] L. Xu,[63a] R. Xu,[131] T. Xu,[108] Y. Xu,[142] Z. Xu,[53] Z. Xu,[114a] B. Yabsley,[151] S. Yacoob,[34a] Y. Yamaguchi,[85] E. Yamashita,[157] H. Yamauchi,[161] T. Yamazaki,[18a] Y. Yamazaki,[86] S. Yan,[60] Z. Yan,[105] H. J. Yang,[63c,63d] H. T. Yang,[63a] S. Yang,[63a] T. Yang,[65c] X. Yang,[37] X. Yang,[14] Y. Yang,[46] Y. Yang,[63a] W-M. Yao,[18a] H. Ye,[56] J. Ye,[14] S. Ye,[30] X. Ye,[63a] Y. Yeh,[98] I. Yeletskikh,[40] B. Yeo,[18b] M. R. Yexley,[98] T. P. Yildirim,[129] P. Yin,[43] K. Yorita,[173] S. Younas,[28b] C. J. S. Young,[37] C. Young,[147] N. D. Young,[126] Y. Yu,[63a] J. Yuan,[14,114c] M. Yuan,[108] R. Yuan,[63d,63c] L. Yue,[98] M. Zaazoua,[63a] B. Zabinski,[88] I. Zahir,[36a] Z. K. Zak,[88] T. Zakareishvili,[168] S. Zambito,[57] J. A. Zamora Saa,[140d,140b] J. Zang,[157] D. Zanzi,[55] R. Zanzottera,[72a,72b] O. Zaplatilek,[135] C. Zeitnitz,[176] H. Zeng,[14] J. C. Zeng,[167] D. T. Zenger Jr.,[27] O. Zenin,[39] T. Ženiš,[29a] S. Zenz,[96] S. Zerradi,[36a] D. Zerwas,[67] M. Zhai,[14,114c] D. F. Zhang,[143] J. Zhang,[63b] J. Zhang,[6] K. Zhang,[14,114c] L. Zhang,[63a] L. Zhang,[114a] P. Zhang,[14,114c] R. Zhang,[175] S. Zhang,[91] T. Zhang,[157] X. Zhang,[63c] Y. Zhang,[142] Y. Zhang,[98] Y. Zhang,[63a] Y. Zhang,[114a] Z. Zhang,[18a] Z. Zhang,[63b] Z. Zhang,[67] H. Zhao,[142] T. Zhao,[63b] Y. Zhao,[35] Z. Zhao,[63a] Z. Zhao,[63a] A. Zhemchugov,[40] J. Zheng,[114a] K. Zheng,[167] X. Zheng,[63a] Z. Zheng,[147] D. Zhong,[167] B. Zhou,[108] H. Zhou,[7] N. Zhou,[63c] Y. Zhou,[15] Y. Zhou,[114a] Y. Zhou,[7] C. G. Zhu,[63b] J. Zhu,[108] X. Zhu,[63d] Y. Zhu,[63c] Y. Zhu,[63a] X. Zhuang,[14] K. Zhukov,[69] N. I. Zimine,[40] J. Zinsser,[64b] M. Ziolkowski,[145] L. Živković,[16] A. Zoccoli,[24b,24a] K. Zoch,[62] T. G. Zorbas,[143] O. Zormpa,[47] W. Zou,[43] and L. Zwalinski[37]

(ATLAS Collaboration)

[1]Department of Physics, University of Adelaide, Adelaide, Australia
[2]Department of Physics, University of Alberta, Edmonton, Alberta, Canada
[3a]Department of Physics, Ankara University, Ankara, Türkiye
[3b]Division of Physics, TOBB University of Economics and Technology, Ankara, Türkiye
[4]LAPP, Université Savoie Mont Blanc, CNRS/IN2P3, Annecy, France
[5]APC, Université Paris Cité, CNRS/IN2P3, Paris, France
[6]High Energy Physics Division, Argonne National Laboratory, Argonne, Illinois, USA
[7]Department of Physics, University of Arizona, Tucson, Arizona, USA
[8]Department of Physics, University of Texas at Arlington, Arlington, Texas, USA
[9]Physics Department, National and Kapodistrian University of Athens, Athens, Greece
[10]Physics Department, National Technical University of Athens, Zografou, Greece
[11]Department of Physics, University of Texas at Austin, Austin, Texas, USA
[12]Institute of Physics, Azerbaijan Academy of Sciences, Baku, Azerbaijan
[13]Institut de Física d'Altes Energies (IFAE), Barcelona Institute of Science and Technology, Barcelona, Spain
[14]Institute of High Energy Physics, Chinese Academy of Sciences, Beijing, China
[15]Physics Department, Tsinghua University, Beijing, China
[16]Institute of Physics, University of Belgrade, Belgrade, Serbia
[17]Department for Physics and Technology, University of Bergen, Bergen, Norway
[18a]Physics Division, Lawrence Berkeley National Laboratory, Berkeley, California, USA

[18b]*University of California, Berkeley, California, USA*

[19]*Institut für Physik, Humboldt Universität zu Berlin, Berlin, Germany*

[20]*Albert Einstein Center for Fundamental Physics and Laboratory for High Energy Physics, University of Bern, Bern, Switzerland*

[21]*School of Physics and Astronomy, University of Birmingham, Birmingham, United Kingdom*

[22a]*Department of Physics, Bogazici University, Istanbul, Türkiye*

[22b]*Department of Physics Engineering, Gaziantep University, Gaziantep, Türkiye*

[22c]*Department of Physics, Istanbul University, Istanbul, Türkiye*

[23a]*Facultad de Ciencias y Centro de Investigaciónes, Universidad Antonio Nariño, Bogotá, Colombia*

[23b]*Departamento de Física, Universidad Nacional de Colombia, Bogotá, Colombia*

[24a]*Dipartimento di Fisica e Astronomia A. Righi, Università di Bologna, Bologna, Italy*

[24b]*INFN Sezione di Bologna, Bologna, Italy*

[25]*Physikalisches Institut, Universität Bonn, Bonn, Germany*

[26]*Department of Physics, Boston University, Boston, Massachusetts, USA*

[27]*Department of Physics, Brandeis University, Waltham, Massachusetts, USA*

[28a]*Transilvania University of Brasov, Brasov, Romania*

[28b]*Horia Hulubei National Institute of Physics and Nuclear Engineering, Bucharest, Romania*

[28c]*Department of Physics, Alexandru Ioan Cuza University of Iasi, Iasi, Romania*

[28d]*National Institute for Research and Development of Isotopic and Molecular Technologies, Physics Department, Cluj-Napoca, Romania*

[28e]*National University of Science and Technology Politechnica, Bucharest, Romania*

[28f]*West University in Timisoara, Timisoara, Romania*

[28g]*Faculty of Physics, University of Bucharest, Bucharest, Romania*

[29a]*Faculty of Mathematics, Physics and Informatics, Comenius University, Bratislava, Slovak Republic*

[29b]*Department of Subnuclear Physics, Institute of Experimental Physics of the Slovak Academy of Sciences, Kosice, Slovak Republic*

[30]*Physics Department, Brookhaven National Laboratory, Upton, New York, USA*

[31]*Universidad de Buenos Aires, Facultad de Ciencias Exactas y Naturales, Departamento de Física, y CONICET, Instituto de Física de Buenos Aires (IFIBA), Buenos Aires, Argentina*

[32]*California State University, Fresno, California, USA*

[33]*Cavendish Laboratory, University of Cambridge, Cambridge, United Kingdom*

[34a]*Department of Physics, University of Cape Town, Cape Town, South Africa*

[34b]*iThemba Labs, Western Cape, South Africa*

[34c]*Department of Mechanical Engineering Science, University of Johannesburg, Johannesburg, South Africa*

[34d]*National Institute of Physics, University of the Philippines Diliman (Philippines), Quezon City, Philippines*

[34e]*University of South Africa, Department of Physics, Pretoria, South Africa*

[34f]*University of Zululand, KwaDlangezwa, South Africa*

[34g]*School of Physics, University of the Witwatersrand, Johannesburg, South Africa*

[35]*Department of Physics, Carleton University, Ottawa, Ontario, Canada*

[36a]*Faculté des Sciences Ain Chock, Université Hassan II de Casablanca, Casablanca, Morocco*

[36b]*Faculté des Sciences, Université Ibn-Tofail, Kénitra, Morocco*

[36c]*Faculté des Sciences Semlalia, Université Cadi Ayyad, LPHEA-Marrakech, Morocco*

[36d]*LPMR, Faculté des Sciences, Université Mohamed Premier, Oujda, Morocco*

[36e]*Faculté des sciences, Université Mohammed V, Rabat, Morocco*

[36f]*Institute of Applied Physics, Mohammed VI Polytechnic University, Ben Guerir, Morocco*

[37]*CERN, Geneva, Switzerland*

[38]*Affiliated with an institute formerly covered by a cooperation agreement with CERN*

[39]*Affiliated with an institute covered by a cooperation agreement with CERN*

[40]*Affiliated with an international laboratory covered by a cooperation agreement with CERN*

[41]*Enrico Fermi Institute, University of Chicago, Chicago, Illinois, USA*

[42]*LPC, Université Clermont Auvergne, CNRS/IN2P3, Clermont-Ferrand, France*

[43]*Nevis Laboratory, Columbia University, Irvington, New York, USA*

[44]*Niels Bohr Institute, University of Copenhagen, Copenhagen, Denmark*

[45a]*Dipartimento di Fisica, Università della Calabria, Rende, Italy*

[45b]*INFN Gruppo Collegato di Cosenza, Laboratori Nazionali di Frascati, Frascati, Italy*

[46]*Physics Department, Southern Methodist University, Dallas, Texas, USA*

[47]*National Centre for Scientific Research "Demokritos", Agia Paraskevi, Greece*

[48a]*Department of Physics, Stockholm University, Stockholm, Sweden*

[48b]*Oskar Klein Centre, Stockholm, Sweden*
[49]*Deutsches Elektronen-Synchrotron DESY, Hamburg and Zeuthen, Germany*
[50]*Fakultät Physik, Technische Universität Dortmund, Dortmund, Germany*
[51]*Institut für Kern- und Teilchenphysik, Technische Universität Dresden, Dresden, Germany*
[52]*Department of Physics, Duke University, Durham, North Carolina, USA*
[53]*SUPA—School of Physics and Astronomy, University of Edinburgh, Edinburgh, United Kingdom*
[54]*INFN e Laboratori Nazionali di Frascati, Frascati, Italy*
[55]*Physikalisches Institut, Albert-Ludwigs-Universität Freiburg, Freiburg, Germany*
[56]*II. Physikalisches Institut, Georg-August-Universität Göttingen, Göttingen, Germany*
[57]*Département de Physique Nucléaire et Corpuscolaire, Université de Genève, Genève, Switzerland*
[58a]*Dipartimento di Fisica, Università di Genova, Genova, Italy*
[58b]*INFN Sezione di Genova, Genova, Italy*
[59]*II. Physikalisches Institut, Justus-Liebig-Universität Giessen, Giessen, Germany*
[60]*SUPA—School of Physics and Astronomy, University of Glasgow, Glasgow, United Kingdom*
[61]*LPSC, Université Grenoble Alpes, CNRS/IN2P3, Grenoble INP, Grenoble, France*
[62]*Laboratory for Particle Physics and Cosmology, Harvard University, Cambridge, Massachusetts, USA*
[63a]*Department of Modern Physics and State Key Laboratory of Particle Detection and Electronics,
University of Science and Technology of China, Hefei, China*
[63b]*Institute of Frontier and Interdisciplinary Science and Key Laboratory of Particle Physics and Particle
Irradiation (MOE), Shandong University, Qingdao, China*
[63c]*School of Physics and Astronomy, Shanghai Jiao Tong University, Key Laboratory for Particle
Astrophysics and Cosmology (MOE), SKLPPC, Shanghai, China*
[63d]*Tsung-Dao Lee Institute, Shanghai, China*
[63e]*School of Physics, Zhengzhou University, Zhengzhou, China*
[64a]*Kirchhoff-Institut für Physik, Ruprecht-Karls-Universität Heidelberg, Heidelberg, Germany*
[64b]*Physikalisches Institut, Ruprecht-Karls-Universität Heidelberg, Heidelberg, Germany*
[65a]*Department of Physics, Chinese University of Hong Kong, Shatin, N.T., Hong Kong, China*
[65b]*Department of Physics, University of Hong Kong, Hong Kong, China*
[65c]*Department of Physics and Institute for Advanced Study, Hong Kong University of Science and
Technology, Clear Water Bay, Kowloon, Hong Kong, China*
[66]*Department of Physics, National Tsing Hua University, Hsinchu, Taiwan*
[67]*IJCLab, Université Paris-Saclay, CNRS/IN2P3, 91405, Orsay, France*
[68]*Centro Nacional de Microelectrónica (IMB-CNM-CSIC), Barcelona, Spain*
[69]*Department of Physics, Indiana University, Bloomington, Indiana, USA*
[70a]*INFN Gruppo Collegato di Udine, Sezione di Trieste, Udine, Italy*
[70b]*ICTP, Trieste, Italy*
[70c]*Dipartimento Politecnico di Ingegneria e Architettura, Università di Udine, Udine, Italy*
[71a]*INFN Sezione di Lecce, Lecce, Italy*
[71b]*Dipartimento di Matematica e Fisica, Università del Salento, Lecce, Italy*
[72a]*INFN Sezione di Milano, Milano, Italy*
[72b]*Dipartimento di Fisica, Università di Milano, Milano, Italy*
[73a]*INFN Sezione di Napoli, Napoli, Italy*
[73b]*Dipartimento di Fisica, Università di Napoli, Napoli, Italy*
[74a]*INFN Sezione di Pavia, Pavia, Italy*
[74b]*Dipartimento di Fisica, Università di Pavia, Pavia, Italy*
[75a]*INFN Sezione di Pisa, Pisa, Italy*
[75b]*Dipartimento di Fisica E. Fermi, Università di Pisa, Pisa, Italy*
[76a]*INFN Sezione di Roma, Roma, Italy*
[76b]*Dipartimento di Fisica, Sapienza Università di Roma, Roma, Italy*
[77a]*INFN Sezione di Roma Tor Vergata, Roma, Italy*
[77b]*Dipartimento di Fisica, Università di Roma Tor Vergata, Roma, Italy*
[78a]*INFN Sezione di Roma Tre, Roma, Italy*
[78b]*Dipartimento di Matematica e Fisica, Università Roma Tre, Roma, Italy*
[79a]*INFN-TIFPA, Povo, Italy*
[79b]*Università degli Studi di Trento, Trento, Italy*
[80]*Universität Innsbruck, Department of Astro and Particle Physics, Innsbruck, Austria*
[81]*University of Iowa, Iowa City, Iowa, USA*
[82]*Department of Physics and Astronomy, Iowa State University, Ames, Iowa, USA*
[83]*Istinye University, Sariyer, Istanbul, Türkiye*

[84a]*Departamento de Engenharia Elétrica, Universidade Federal de Juiz de Fora (UFJF),
Juiz de Fora, Brazil*
[84b]*Universidade Federal do Rio De Janeiro COPPE/EE/IF, Rio de Janeiro, Brazil*
[84c]*Instituto de Física, Universidade de São Paulo, São Paulo, Brazil*
[84d]*Rio de Janeiro State University, Rio de Janeiro, Brazil*
[84e]*Federal University of Bahia, Bahia, Brazil*
[85]*KEK, High Energy Accelerator Research Organization, Tsukuba, Japan*
[86]*Graduate School of Science, Kobe University, Kobe, Japan*
[87a]*AGH University of Krakow, Faculty of Physics and Applied Computer Science, Krakow, Poland*
[87b]*Marian Smoluchowski Institute of Physics, Jagiellonian University, Krakow, Poland*
[88]*Institute of Nuclear Physics Polish Academy of Sciences, Krakow, Poland*
[89]*Faculty of Science, Kyoto University, Kyoto, Japan*
[90]*Research Center for Advanced Particle Physics and Department of Physics, Kyushu University,
Fukuoka, Japan*
[91]*L2IT, Université de Toulouse, CNRS/IN2P3, UPS, Toulouse, France*
[92]*Instituto de Física La Plata, Universidad Nacional de La Plata and CONICET, La Plata, Argentina*
[93]*Physics Department, Lancaster University, Lancaster, United Kingdom*
[94]*Oliver Lodge Laboratory, University of Liverpool, Liverpool, United Kingdom*
[95]*Department of Experimental Particle Physics, Jožef Stefan Institute and Department of Physics,
University of Ljubljana, Ljubljana, Slovenia*
[96]*School of Physics and Astronomy, Queen Mary University of London, London, United Kingdom*
[97]*Department of Physics, Royal Holloway University of London, Egham, United Kingdom*
[98]*Department of Physics and Astronomy, University College London, London, United Kingdom*
[99]*Louisiana Tech University, Ruston, Louisiana, USA*
[100]*Fysiska institutionen, Lunds universitet, Lund, Sweden*
[101]*Departamento de Física Teorica C-15 and CIAFF, Universidad Autónoma de Madrid, Madrid, Spain*
[102]*Institut für Physik, Universität Mainz, Mainz, Germany*
[103]*School of Physics and Astronomy, University of Manchester, Manchester, United Kingdom*
[104]*CPPM, Aix-Marseille Université, CNRS/IN2P3, Marseille, France*
[105]*Department of Physics, University of Massachusetts, Amherst, Massachusetts, USA*
[106]*Department of Physics, McGill University, Montreal, Quebec, Canada*
[107]*School of Physics, University of Melbourne, Victoria, Australia*
[108]*Department of Physics, University of Michigan, Ann Arbor, Michigan, USA*
[109]*Department of Physics and Astronomy, Michigan State University, East Lansing, Michigan, USA*
[110]*Group of Particle Physics, University of Montreal, Montreal, Quebec, Canada*
[111]*Fakultät für Physik, Ludwig-Maximilians-Universität München, München, Germany*
[112]*Max-Planck-Institut für Physik (Werner-Heisenberg-Institut), München, Germany*
[113]*Graduate School of Science and Kobayashi-Maskawa Institute, Nagoya University, Nagoya, Japan*
[114a]*Department of Physics, Nanjing University, Nanjing, China*
[114b]*School of Science, Shenzhen Campus of Sun Yat-sen University, Shenzhen, China*
[114c]*University of Chinese Academy of Science (UCAS), Beijing, China*
[115]*Department of Physics and Astronomy, University of New Mexico, Albuquerque, New Mexico, USA*
[116]*Institute for Mathematics, Astrophysics and Particle Physics, Radboud University/Nikhef,
Nijmegen, Netherlands*
[117]*Nikhef National Institute for Subatomic Physics and University of Amsterdam, Amsterdam, Netherlands*
[118]*Department of Physics, Northern Illinois University, DeKalb, Illinois, USA*
[119a]*New York University Abu Dhabi, Abu Dhabi, United Arab Emirates*
[119b]*United Arab Emirates University, Al Ain, United Arab Emirates*
[120]*Department of Physics, New York University, New York, New York, USA*
[121]*Ochanomizu University, Otsuka, Bunkyo-ku, Tokyo, Japan*
[122]*Ohio State University, Columbus, Ohio, USA*
[123]*Homer L. Dodge Department of Physics and Astronomy, University of Oklahoma,
Norman, Oklahoma, USA*
[124]*Department of Physics, Oklahoma State University, Stillwater, Oklahoma, USA*
[125]*Palacký University, Joint Laboratory of Optics, Olomouc, Czech Republic*
[126]*Institute for Fundamental Science, University of Oregon, Eugene, Oregon, USA*
[127]*Graduate School of Science, Osaka University, Osaka, Japan*
[128]*Department of Physics, University of Oslo, Oslo, Norway*
[129]*Department of Physics, Oxford University, Oxford, United Kingdom*
[130]*LPNHE, Sorbonne Université, Université Paris Cité, CNRS/IN2P3, Paris, France*

[131]Department of Physics, University of Pennsylvania, Philadelphia, Pennsylvania, USA

[132]Department of Physics and Astronomy, University of Pittsburgh, Pittsburgh, Pennsylvania, USA

[133a]Laboratório de Instrumentação e Física Experimental de Partículas—LIP, Lisboa, Portugal

[133b]Departamento de Física, Faculdade de Ciências, Universidade de Lisboa, Lisboa, Portugal

[133c]Departamento de Física, Universidade de Coimbra, Coimbra, Portugal

[133d]Centro de Física Nuclear da Universidade de Lisboa, Lisboa, Portugal

[133e]Departamento de Física, Universidade do Minho, Braga, Portugal

[133f]Departamento de Física Teórica y del Cosmos, Universidad de Granada, Granada (Spain), Spain

[133g]Departamento de Física, Instituto Superior Técnico, Universidade de Lisboa, Lisboa, Portugal

[134]Institute of Physics of the Czech Academy of Sciences, Prague, Czech Republic

[135]Czech Technical University in Prague, Prague, Czech Republic

[136]Charles University, Faculty of Mathematics and Physics, Prague, Czech Republic

[137]Particle Physics Department, Rutherford Appleton Laboratory, Didcot, United Kingdom

[138]IRFU, CEA, Université Paris-Saclay, Gif-sur-Yvette, France

[139]Santa Cruz Institute for Particle Physics, University of California Santa Cruz,
Santa Cruz, California, USA

[140a]Departamento de Física, Pontificia Universidad Católica de Chile, Santiago, Chile

[140b]Millennium Institute for Subatomic physics at high energy frontier (SAPHIR), Santiago, Chile

[140c]Instituto de Investigación Multidisciplinario en Ciencia y Tecnología, y Departamento de Física,
Universidad de La Serena, Chile

[140d]Universidad Andres Bello, Department of Physics, Santiago, Chile

[140e]Instituto de Alta Investigación, Universidad de Tarapacá, Arica, Chile

[140f]Departamento de Física, Universidad Técnica Federico Santa María, Valparaíso, Chile

[141]Department of Physics, Institute of Science, Tokyo, Japan

[142]Department of Physics, University of Washington, Seattle, Washington, USA

[143]Department of Physics and Astronomy, University of Sheffield, Sheffield, United Kingdom

[144]Department of Physics, Shinshu University, Nagano, Japan

[145]Department Physik, Universität Siegen, Siegen, Germany

[146]Department of Physics, Simon Fraser University, Burnaby, British Columbia, Canada

[147]SLAC National Accelerator Laboratory, Stanford, California, USA

[148]Department of Physics, Royal Institute of Technology, Stockholm, Sweden

[149]Departments of Physics and Astronomy, Stony Brook University, Stony Brook, New York, USA

[150]Department of Physics and Astronomy, University of Sussex, Brighton, United Kingdom

[151]School of Physics, University of Sydney, Sydney, Australia

[152]Institute of Physics, Academia Sinica, Taipei, Taiwan

[153a]E. Andronikashvili Institute of Physics, Iv. Javakhishvili Tbilisi State University, Tbilisi, Georgia

[153b]High Energy Physics Institute, Tbilisi State University, Tbilisi, Georgia

[153c]University of Georgia, Tbilisi, Georgia

[154]Department of Physics, Technion, Israel Institute of Technology, Haifa, Israel

[155]Raymond and Beverly Sackler School of Physics and Astronomy, Tel Aviv University, Tel Aviv, Israel

[156]Department of Physics, Aristotle University of Thessaloniki, Thessaloniki, Greece

[157]International Center for Elementary Particle Physics and Department of Physics, University of Tokyo,
Tokyo, Japan

[158]Graduate School of Science and Technology, Tokyo Metropolitan University, Tokyo, Japan

[159]Department of Physics, University of Toronto, Toronto, Ontario, Canada

[160a]TRIUMF, Vancouver, British Columbia, Canada

[160b]Department of Physics and Astronomy, York University, Toronto, Ontario, Canada

[161]Division of Physics and Tomonaga Center for the History of the Universe, Faculty of Pure and Applied
Sciences, University of Tsukuba, Tsukuba, Japan

[162]Department of Physics and Astronomy, Tufts University, Medford, Massachusetts, USA

[163]Department of Physics and Astronomy, University of California Irvine, Irvine, California, USA

[164]University of West Attica, Athens, Greece

[165]University of Sharjah, Sharjah, United Arab Emirates

[166]Department of Physics and Astronomy, University of Uppsala, Uppsala, Sweden

[167]Department of Physics, University of Illinois, Urbana, Illinois, USA

[168]Instituto de Física Corpuscular (IFIC), Centro Mixto Universidad de Valencia—CSIC, Valencia, Spain

[169]Department of Physics, University of British Columbia, Vancouver, British Columbia, Canada

[170]Department of Physics and Astronomy, University of Victoria, Victoria, British Columbia, Canada

[171]Fakultät für Physik und Astronomie, Julius-Maximilians-Universität Würzburg, Würzburg, Germany

[172]Department of Physics, University of Warwick, Coventry, United Kingdom

[173]*Waseda University, Tokyo, Japan*
[174]*Department of Particle Physics and Astrophysics, Weizmann Institute of Science, Rehovot, Israel*
[175]*Department of Physics, University of Wisconsin, Madison, Wisconsin, USA*
[176]*Fakultät für Mathematik und Naturwissenschaften, Fachgruppe Physik,*
Bergische Universität Wuppertal, Wuppertal, Germany
[177]*Department of Physics, Yale University, New Haven, Connecticut, USA*
[178]*Yerevan Physics Institute, Yerevan, Armenia*

[a]Deceased.
[b]Also at Department of Physics, King's College London, London, United Kingdom.
[c]Also at Institute of Physics, Azerbaijan Academy of Sciences, Baku, Azerbaijan.
[d]Also at Imam Mohammad Ibn Saud Islamic University, Saudi Arabia.
[e]Also at TRIUMF, Vancouver, British Columbia, Canada.
[f]Also at Department of Physics, University of Thessaly, Greece.
[g]Also at An-Najah National University, Nablus, Palestine.
[h]Also at Department of Physics, University of Fribourg, Fribourg, Switzerland.
[i]Also at Department of Physics, Westmont College, Santa Barbara, USA.
[j]Also at Departament de Fisica de la Universitat Autonoma de Barcelona, Barcelona, Spain.
[k]Also at Affiliated with an institute covered by a cooperation agreement with CERN.
[l]Also at The Collaborative Innovation Center of Quantum Matter (CICQM), Beijing, China.
[m]Also at Faculty of Physics, Sofia University, 'St. Kliment Ohridski', Sofia, Bulgaria.
[n]Also at Università di Napoli Parthenope, Napoli, Italy.
[o]Also at Institute of Particle Physics (IPP), Canada.
[p]Also at Department of Physics, Bolu Abant Izzet Baysal University, Bolu, Türkiye.
[q]Also at Borough of Manhattan Community College, City University of New York, New York, New York, USA.
[r]Also at National Institute of Physics, University of the Philippines Diliman (Philippines), Philippines.
[s]Also at Department of Financial and Management Engineering, University of the Aegean, Chios, Greece.
[t]Also at Institucio Catalana de Recerca i Estudis Avancats, ICREA, Barcelona, Spain.
[u]Also at Henan University, China.
[v]Also at Technical University of Munich, Munich, Germany.
[w]Also at CMD-AC UNEC Research Center, Azerbaijan State University of Economics (UNEC), Azerbaijan.
[x]Also at Yeditepe University, Physics Department, Istanbul, Türkiye.
[y]Also at CERN, Geneva, Switzerland.
[z]Also at Center for Interdisciplinary Research and Innovation (CIRI-AUTH), Thessaloniki, Greece.
[aa]Also at University of the Western Cape, South Africa.
[bb]Also at Hellenic Open University, Patras, Greece.
[cc]Also at Center for High Energy Physics, Peking University, China.
[dd]Also at Department of Mathematical Sciences, University of South Africa, Johannesburg, South Africa.
[ee]Also at Department of Physics, Stellenbosch University, South Africa.
[ff]Also at Department of Physics, California State University, Sacramento, United States of America.
[gg]Also at University of Colorado Boulder, Department of Physics, Colorado, USA.
[hh]Also at Département de Physique Nucléaire et Corpusculaire, Université de Genève, Genève, Switzerland.
[ii]Also at Institut für Experimentalphysik, Universität Hamburg, Hamburg, Germany.
[jj]Also at Institute for Nuclear Research and Nuclear Energy (INRNE) of the Bulgarian Academy of Sciences, Sofia, Bulgaria.
[kk]Also at Washington College, Chestertown, Maryland, USA.
[ll]Also at Institute of Applied Physics, Mohammed VI Polytechnic University, Ben Guerir, Morocco.
[mm]Also at Department of Physics, Stanford University, Stanford, California, USA.